

Semiparametric spectral modeling of the *Drosophila* connectome

C.E. Priebe, Y. Park, M. Tang, A. Athreya, V. Lyzinski, J.T. Vogelstein
Johns Hopkins University

Yichen Qin
University of Cincinnati

Ben Cocanougher
HHMI Janelia Research Campus & Cambridge University, UK

Katharina Eichler
HHMI Janelia Research Campus & University of Konstanz, Germany

Marta Zlatic and Albert Cardona
HHMI Janelia Research Campus

May 10, 2017

Abstract

We present semiparametric spectral modeling of the complete larval *Drosophila* mushroom body connectome. Motivated by a thorough exploratory data analysis of the network via Gaussian mixture modeling (GMM) in the adjacency spectral embedding (ASE) representation space, we introduce the *latent structure model* (LSM) for network modeling and inference. LSM is a generalization of the stochastic block model (SBM) and a special case of the random dot product graph (RDPG) latent position model, and is amenable to semiparametric GMM in the ASE representation space. The resulting *connectome code* derived via semiparametric GMM composed with ASE captures latent connectome structure and elucidates biologically relevant neuronal properties.

Keywords: Connectome; Network; Graph; Spectral embedding; Mixture model; Clustering; Latent structure model (LSM)

1 Introduction: Brains & connectomes

The term “connectome” was coined by Hagmann (2005) and Sporns et al. (2005), and has come to mean any “brain graph”; “connectomics” means the study of such graphs; and “statistical connectomics” means the statistical analysis of such graphs.

The Human Connectome Project (<http://www.humanconnectomeproject.org>) “aims to provide an unparalleled compilation of neural data, an interface to graphically navigate this data and the opportunity to achieve never before realized conclusions about the living human brain.” Sporns (2012) provides a recent survey of the quest to discover the human connectome. Glasser et al. (2016) presents the newest results in the long history of efforts to update the Brodmann region atlas (Zilles and Amunts, 2010).

There are various connectomes available, including at the macro-scale connectomes constructed from structural, functional, and diffusion MRI data. For instance, the Open Connectome Project (<http://www.openconnectomeproject.org>) makes available connectomes collected via structural magnetic resonance imaging (MRI), functional MRI (fMRI), diffusion tensor imaging (DTI), and diffusion spectrum imaging (DSI). These macro-scale connectomes are used, for example, to investigate connectivity between (sub)cortical regions.

In addition to MRI modalities, there are behavioral connectomes (via optogenetics), activity-based connectomes (via calcium imaging), etc. For example, Ko et al. (2011) and Lee et al. (2016) consider activity-based connectomes, and Vogelstein et al. (2014) investigates a behavioral connectome obtained via optogenetic neuron manipulation.

At the neurons-as-vertices and synapses-as-edges scale, partial connectomes of various organisms (*C. elegans*, *Drosophila*, zebrafish, mouse, etc.) are also available. The full connectome of the roundworm *C. elegans* has been made available at this micro-scale via electron microscopy (White et al., 1986, Varshney et al., 2011). This data continues to be widely studied. Notably, there are *two* connectomes available for *C. elegans* – one based on chemical synapses and one based on electrical synapses; Chen et al. (2016) presents a joint graph inference case study of the *C. elegans* chemical and electrical connectomes.

A holy grail of connectomics is the “connectome code” – a generative model characterizing important aspects of the connectome¹. This paper reports the results of a “structure discovery” analysis of an important first-of-its-kind complete neurons-as-vertices and synapses-as-edges electron microscopy connectome. The paper is organized as follows. Section 2 provides a brief description of our data, the larval *Drosophila* mushroom body connectome described in detail in Eichler et al. (2017). Section 3 presents a thorough spectral clustering investigation of this connectome, demonstrating conclusively that there is one major aspect of the connectome that is insufficiently captured by this approach. Section 4 introduces and develops the principled semiparametric spectral modeling methodology that we use to generate a much more satisfying connectome code for the larval *Drosophila* mushroom body. Section 5 provides both neuroscientific and methodological discussion, and Section 6 presents our conclusion. Algorithmic details are provided in an appendix.

2 The larval *Drosophila* mushroom body connectome

HHMI Janelia recently reconstructed the complete wiring diagram of the higher order parallel fiber system for associative learning in the larval *Drosophila* brain, the mushroom body (MB). Memories are thought to be stored as functional and structural changes in connections between neurons, but the complete circuit architecture of a higher-order learning center involved in memory formation or storage has not been known in any organism ... until now. This data set provides a real and important example for initial investigation into synapse-level structural connectome modeling.

The MB connectome was obtained via serial section transmission electron microscopy of an

¹ Neural coding characterizes the relationship between the ongoing external environment (stimuli or behaviors) and neural activity. By way of analogy, connectome coding characterizes the relationship between past experience (including genetics) and neural connectivity. Specifically, which properties of connectomes are preserved across individuals of the same species, and which vary as a function of life history? Similarly, which connectome codes are preserved across species, and which are adapted to species’ specific evolutionary niches?

entire larval *Drosophila* nervous system (Ohyama et al., 2015, Schneider-Mizell et al., 2016). This connectome contains the entirety of MB intrinsic neurons called Kenyon cells and all of their pre- and post-synaptic partners (Eichler et al., 2017).

We consider the right hemisphere MB. The connectome consists of four distinct types of neurons – Kenyon Cells (KC), Input Neurons (MBIN), Output Neurons (MBON), Projection Neurons (PN) – with directed connectivity illustrated in Figure 1. There are $n = 213$ neurons², with $n_{KC} = 100$, $n_{MBIN} = 21$, $n_{MBON} = 29$, and $n_{PN} = 63$. Figure 2 displays the observed MB connectome as an adjacency matrix. Note that, in accordance with Figure 1, Figure 2 shows data (edges) in only eight of the 16 blocks. cir

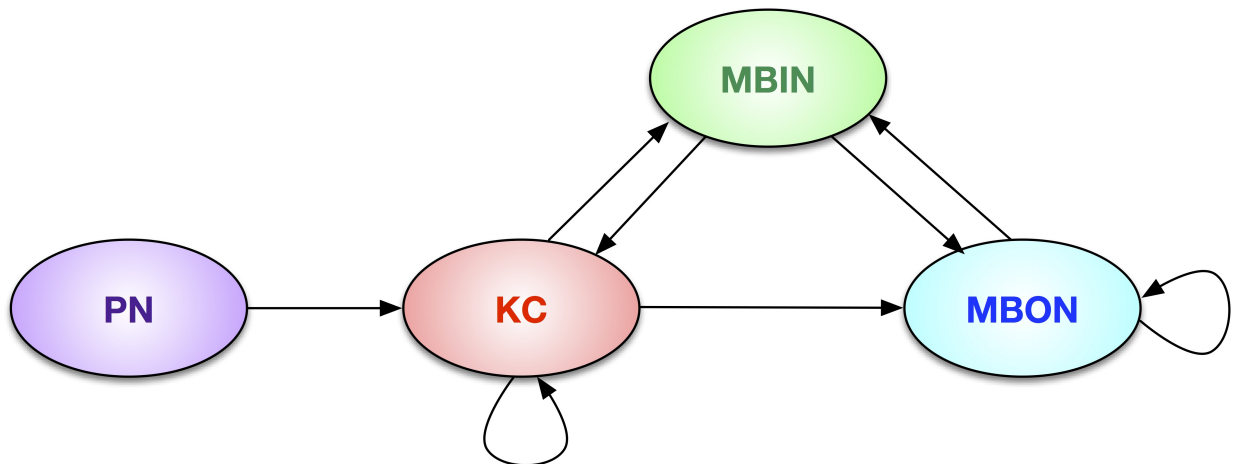


Figure 1: Illustration of the larval *Drosophila* mushroom body connectome as a directed graph on four neuron types.

² There are 13 isolates, all are KC; removing these isolates makes the (directed) graph one (weakly, but not strongly) connected component with 213 vertices and 7536 directed edges.

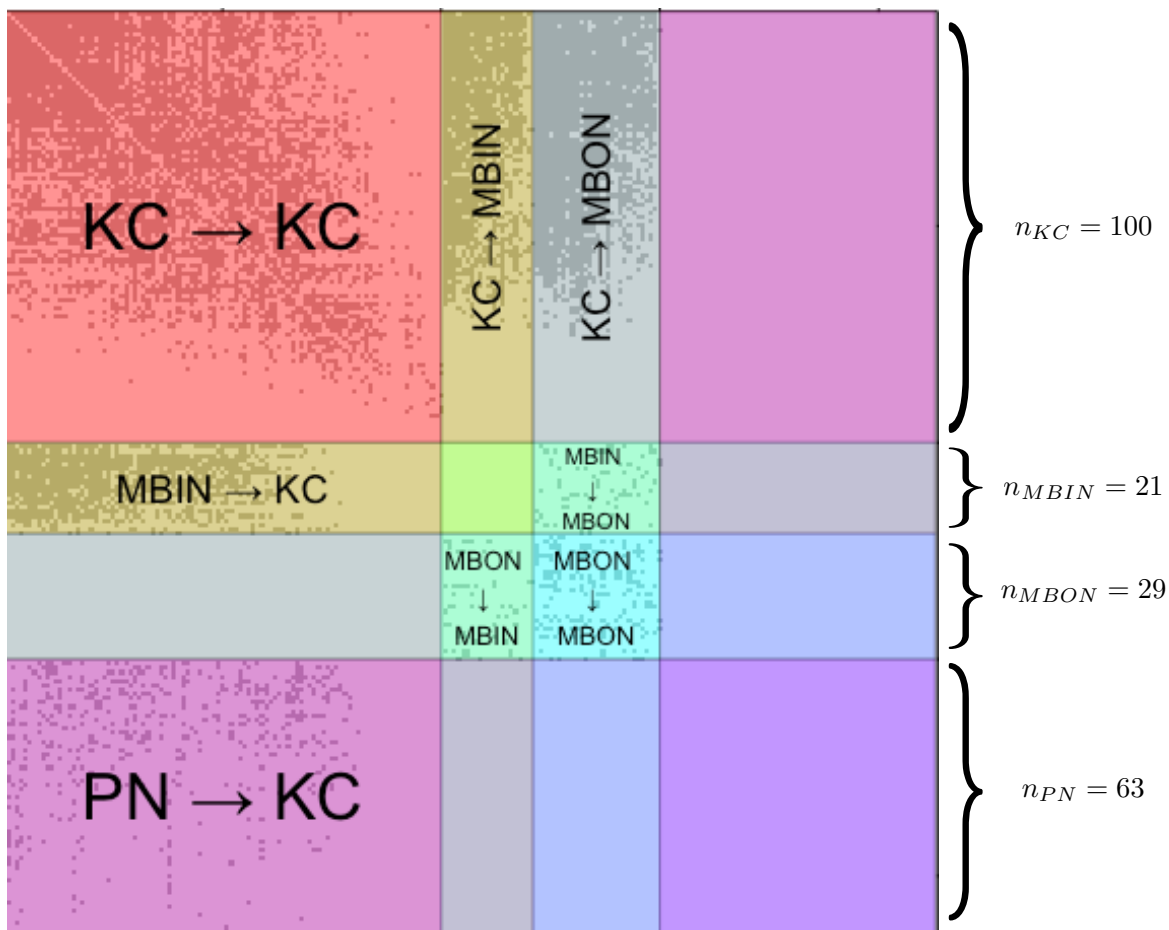


Figure 2: Observed data for the MB connectome as a directed adjacency matrix on four neuron types with 213 vertices ($n_{KC} = 100$, $n_{MBIN} = 21$, $n_{MBON} = 29$, and $n_{PN} = 63$) and 7536 directed edges.

3 Spectral clustering

Due to its undeniable four-neuron-type connectivity structure, we might think of the MB connectome, to first order, as an observation from a ($K = 4$)-block directed stochastic block model (SBM) on n vertices. (The SBM was introduced in Holland et al. (1983); the directed version in Wang and Wong (1987).) This model is parameterized by (*i*) a block membership

probability vector $\rho = [\rho_1, \dots, \rho_K]$ such that $\rho_k \geq 0$ for all k and $\sum_k \rho_k = 1$ and (ii) a $K \times K$ block connectivity probability matrix B with entries $B_{k_1, k_2} \in [0, 1]$ governing the probability of directed edges from vertices in block k_1 to vertices in block k_2 . For this model of the MB connectome we have

$$B = \begin{bmatrix} B_{11} & B_{12} & B_{13} & 0 \\ B_{21} & 0 & B_{23} & 0 \\ 0 & B_{32} & B_{33} & 0 \\ B_{41} & 0 & 0 & 0 \end{bmatrix}$$

where the 0 in the B_{31} entry, for example, indicates that there are no directed connections from any MBON neuron to any KC neuron (as seen in Figures 1 and 2).

Theory and methods suggest Gaussian mixture modeling (see, for example, Fraley and Raftery (2002)) composed with adjacency spectral embedding (see, for example, Sussman et al. (2012)), denoted $GMM \circ ASE$, for analysis of the (directed) SBM³.

Adjacency spectral embedding (ASE) of a directed graph on n vertices (e.g., the MB connectome with $n = 213$ neurons, depicted as a directed adjacency matrix in Figure 2) employs the singular value decomposition (SVD) to represent the $n \times n$ adjacency matrix via $A = USV^T$ and chooses the top d singular values and their associated left- and right-singular vectors to embed the graph as n points in \mathbb{R}^{2d} via the concatenation

$$\widehat{X} = \left[U_d S_d^{1/2} \mid V_d S_d^{1/2} \right] \in \mathbb{R}^{n \times 2d}.$$

(The scaled left-singular vectors $U_d S_d^{1/2}$ are interpreted as the “out-vector” representation of the digraph, modeling vertices’ propensity to originate directed edges; similarly, $V_d S_d^{1/2}$ are interpreted as the “in-vectors”.) Gaussian mixture modeling (GMM) then fits a K -component $2d$ -dimensional Gaussian mixture model to the points $\widehat{X}_1, \dots, \widehat{X}_n$ given by the rows of \widehat{X} .

³ $GMM \circ ASE$ for directed SBM: the ASE CLT (Athreya et al., 2016) suggests (mutatis mutandis) that concatenation of the top K left/right singular vectors from a directed K -SBM adjacency matrix behaves approximately as a random sample from a mixture of K Gaussians in \mathbb{R}^{2K} . Tang and Priebe (2016) demonstrates that the choice between adjacency spectral embedding and Laplacian spectral embedding is an empirical modeling issue as neither dominates the other for subsequent inference ... and that K -means is inferior to GMM for spectral clustering.

If the graph is an SBM (or indeed more generally) then $GMM \circ ASE$ provides consistent subsequent inference (Sussman et al., 2012, Fishkind et al., 2013, Tang et al., 2013, Sussman et al., 2014, Lyzinski et al., 2014, 2017, Athreya et al., 2016, Tang and Priebe, 2016).

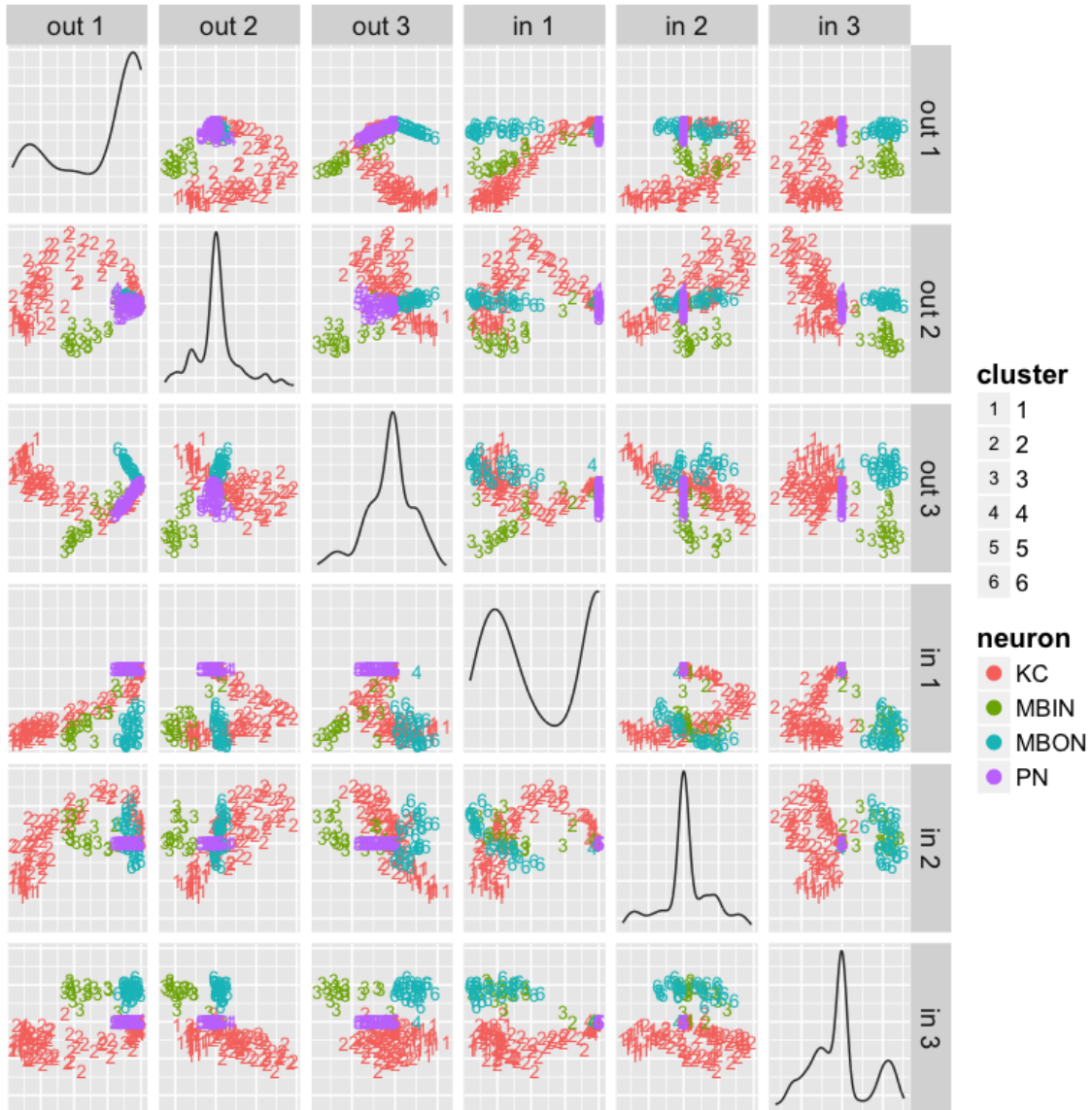


Figure 3: Pairs plot for the clustered embedding of the MB connectome into $\hat{d} = 6$ dimensions with $\hat{K} = 6$ clusters. The cluster confusion matrix with respect to true neuron types is presented in Table 1.

$GMM \circ ASE$ applied to the MB connectome yields the clustered embedding depicted via the pairs plot presented in Figure 3, with the associated cluster confusion matrix with respect to true neuron types presented in Table 1. The clusters are clearly coherent with the four true neuron types. (For ease of illustration, Figure 4 presents just the out1 vs. out2 subspace.)

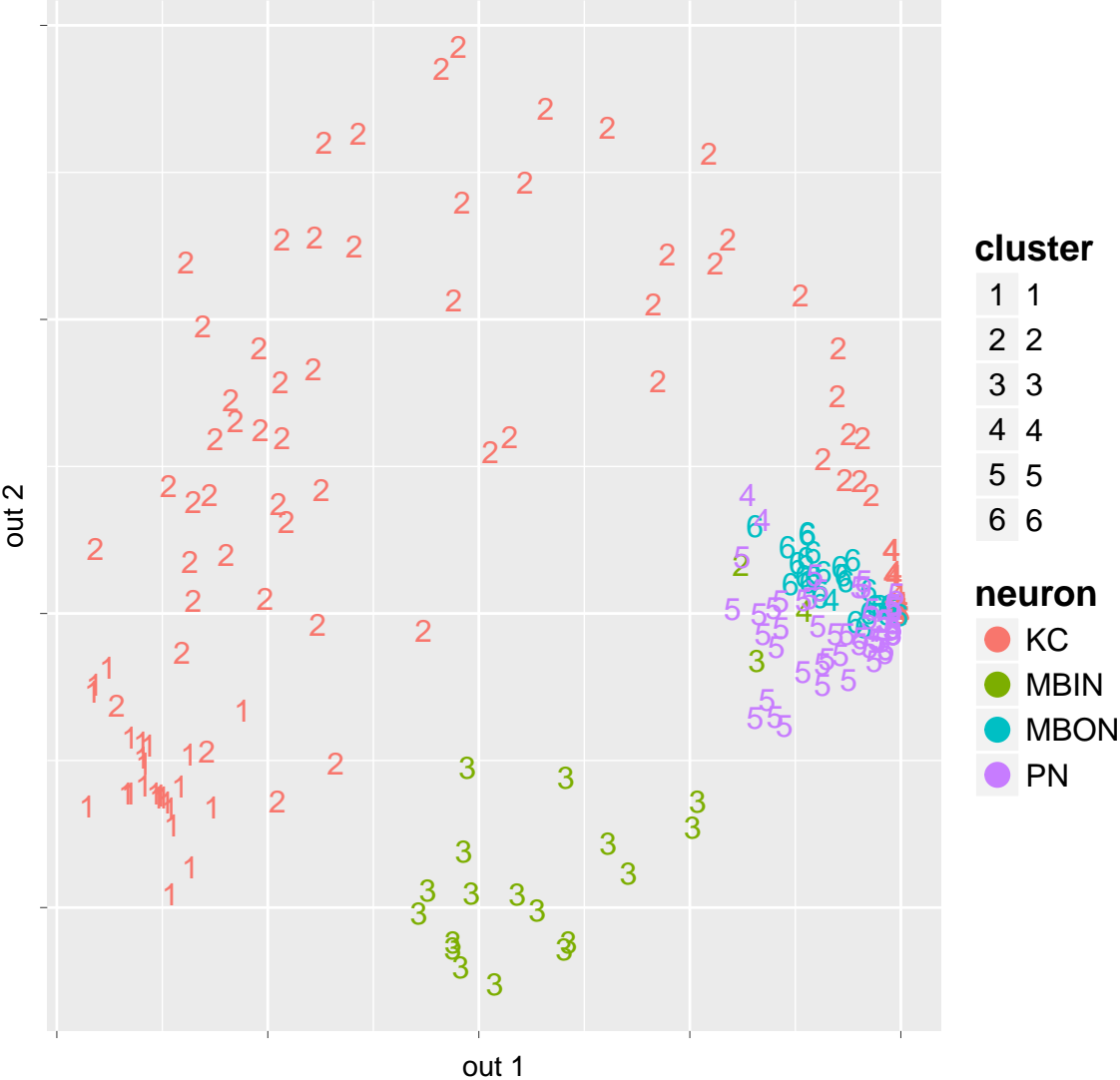


Figure 4: Plot for the clustered embedding of the MB connectome in the out1 vs. out2 dimensions. For ease of illustration, we present embedding results in this two-dimensional subspace throughout the remainder of this manuscript. Recall that this is a two-dimensional visualization of six-dimensional structure.

There are two model selection problems inherent in spectral clustering in general, and in obtaining our $GMM \circ ASE$ clustered embedding (Figure 3) in particular: choice of embedding dimension (\hat{d}), and choice of mixture complexity (\hat{K}).

A ubiquitous and principled method for choosing the number of dimensions in eigendecompositions and SVDs (e.g., principal components analysis, factor analysis, spectral embedding, etc.) is to examine the so-called scree plot (the SVD scree plot for our MB connectome is presented in Figure 5) and look for “elbows” or “knees” defining the cut-off between the top (signal) dimensions and the noise dimensions. Identifying a “best” method is, in general, impossible, as the bias-variance tradeoff demonstrates that, for small n , subsequent inference may be optimized by choosing a dimension *smaller than* the true signal dimension; see Section 3 of Jain et al. (2000) for a clear and concise illustration of this phenomenon. There are a plethora of variations for automating this singular value thresholding (SVT); Section 2.8 of Jackson (2004) provides a comprehensive discussion in the context of principal components, and Chatterjee (2015) provides a theoretically-justified (but perhaps practically suspect, for small n) universal SVT. Using the profile likelihood SVT method of Zhu and Ghodsi (2006) yields a cut-off at three singular values, as depicted in Figure 5. Recall that, as this is a directed graph, we have both left- & right-singular vectors for each vertex; thus the SVT choice of three singular values results in $\hat{d} = 6$.

Similarly, a ubiquitous and principled method for choosing the number of clusters in, for example, Gaussian mixture models, is to maximize a fitness criterion penalized by model complexity. Common approaches include Akaike Information Criterion (AIC) (Akaike, 1974), Bayesian Information Criterion (BIC) (Schwarz, 1978), Minimum Description Length (MDL) (Rissanen, 1978), etc. Again, identifying a “best” method is, in general, impossible, as the bias-variance tradeoff demonstrates that, for small n , inference performance may be optimized by choosing a number of clusters *smaller than* the true cluster complexity; see for example Bickel and Doksum (2007) Problem 6.6.8. MCLUST’s BIC (Fraley and Raftery, 2002) applied to our MB connectome embedded via ASE into $\mathbb{R}^{\hat{d}=6}$ is maximized at six clusters, as depicted in Figure 6, and hence $\hat{K} = 6$. (MCLUST’s most general covariance model – “VVV” = ellipsoidal with varying volume, shape, and orientation – is the winner.)

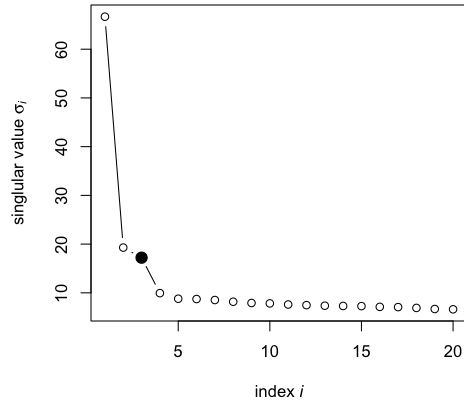


Figure 5: Model Selection: embedding dimension $\hat{d} = 6$ – the top 3 singular values and their associated left- and right-singular vectors – is chosen by SVT.

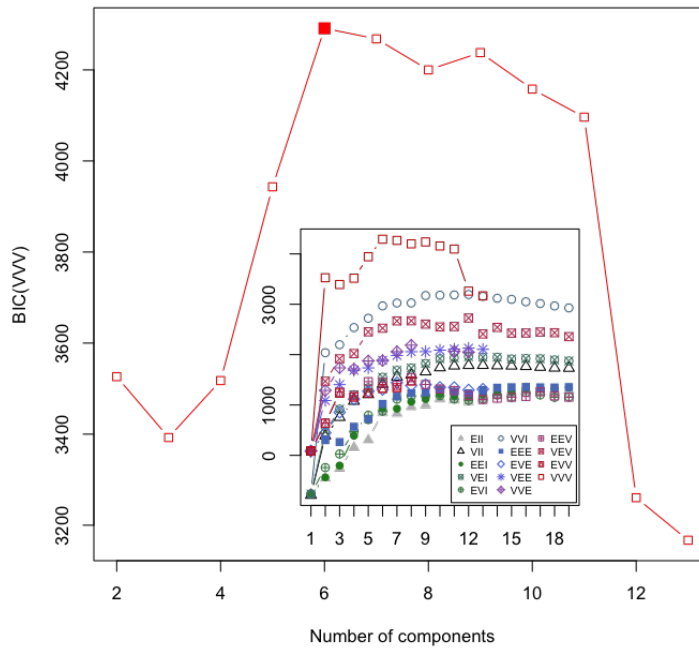


Figure 6: Model Selection: mixture complexity $\hat{K} = 6$ is chosen by BIC. (The inset shows that the main curve – BIC for dimensions 2 through 13 for MCLUST’s most general covariance model, in red – dominates all other dimensions and all other models.)

The $\hat{K} = 6$ clusters reported in Table 1 are essentially correct, with just a few misclustered neurons – e.g., cluster #3 contains only MBIN and most of the MBIN, cluster #5 contains mostly PN and most of the PN, and cluster #6 contains only MBON and most of the MBON – and, notably, KC being distributed across multiple clusters.

	1	2	3	4	5	6
KC	25	57	0	16	2	0
MBIN	0	1	19	1	0	0
MBON	0	0	0	1	0	28
PN	0	0	0	2	61	0

Table 1: $GMM \circ ASE$ for our MB connectome yields $\hat{K} = 6$ clusters. The clusters are clearly coherent with but not perfectly aligned with the four true neuron types, as presented in this confusion matrix.

While BIC chooses $\hat{K} = 6$ clusters, it is natural to ask whether the distribution of KC across multiple clusters is an artifact of insufficiently parsimonious model selection. However, choosing four or five clusters not only (substantially) decreases BIC, but in fact leaves KC distributed across multiple clusters while splitting and/or merging other neuron types. In the direction of less parsimony, Figure 6 suggests that any choice from 7 to 11 clusters is competitive, in terms of BIC, with the maximizer $\hat{K} = 6$. Moreover, any of these choices only slightly decreases BIC, while leaving PN, MBIN, and MBON clustered (mostly) singularly and (mostly) purely and distributing KC across more clusters. Tables 2, 3, and 4 show cluster confusion matrices for other choices of K .

	1	2	3	4
KC	26	56	16	2
MBIN	0	20	1	0
MBON	0	28	1	0
PN	0	0	16	47

Table 2: Cluster confusion matrix for $GMM \circ ASE$ with 4 clusters. Choosing four or five clusters not only (substantially) decreases BIC (compared to $\hat{K} = 6$), but in fact leaves KC distributed across multiple clusters while splitting and/or merging other neuron types.

	1	2	3	4	5
KC	26	56	16	2	0
MBIN	0	20	1	0	0
MBON	0	0	1	0	28
PN	0	0	16	47	0

Table 3: Cluster confusion matrix for $GMM \circ ASE$ with 5 clusters. Choosing four or five clusters not only (substantially) decreases BIC (compared to $\hat{K} = 6$), but in fact leaves KC distributed across multiple clusters while splitting and/or merging other neuron types.

	1	2	3	4	5	6	7
KC	25	42	15	0	16	2	0
MBIN	0	0	1	19	1	0	0
MBON	0	0	0	0	1	0	28
PN	0	0	0	0	2	61	0

Table 4: Cluster confusion matrix for $GMM \circ ASE$ with 7 clusters. Any choice from 7 to 11 clusters only slightly decreases BIC (compared to $\hat{K} = 6$), while leaving PN, MBIN, and MBON clustered (mostly) singularly and (mostly) purely and distributing KC across more clusters.

We perform a cluster assessment to investigate the (unsupervised) selection of $\hat{K} = 6$ via BIC and $\hat{d} = 6$ via SVT in terms of the true neuron types. There are numerous cluster assessment criteria available in the literature; we consider Adjusted Rand Index (ARI) (Hubert and Arabie, 1985), Normalized Mutual Information (NMI) (Danon et al., 2005), Variation of Information (VI) (Meilă, 2007), and Jaccard (Jaccard, 1912). (For all but VI, bigger is better; ergo, we report $1/\text{VI}$ for convenience.) In Table 5 we fix $\hat{d} = 6$ and show that BIC’s $\hat{K} = 6$ coincides with the best choice of mixture complexity. In Table 6 we find the best clustering in various embedding dimensions and show that SVT’s $\hat{d} = 6$ coincides with a fine choice of embedding dimension – choosing 4 dimensions seems approximately as good for the subsequent clustering task, while choosing 2 or 8 dimensions yields degraded performance.

	ARI	NMI	1/VI	Jaccard
4	0.26	0.44	0.73	0.34
5	0.43	0.60	0.92	0.41
$\hat{K} = 6$	0.63	0.75	1.39	0.57
7	0.55	0.72	1.15	0.49
8	0.49	0.68	0.99	0.43
9	0.49	0.68	0.96	0.42
10	0.46	0.66	0.88	0.40
11	0.45	0.65	0.84	0.39

Table 5: Clustering analyzed in terms of the true neuron types (bigger is better) shows that the (unsupervised) selection of $\hat{K} = 6$ via BIC coincides with the objectively best clustering.

	ARI	NMI	1/VI	Jaccard
2	0.61	0.71	1.19	0.34
4	0.60	0.76	1.43	0.34
$\hat{d} = 6$	0.63	0.75	1.39	0.35
8	0.41	0.67	0.91	0.30

Table 6: Dimension selection analyzed in terms of the true neuron types (bigger is better) shows that the (unsupervised) selection of $\hat{d} = 6$ via SVT coincides with a fine choice of embedding dimension – choosing 4 dimensions seems approximately as good for the subsequent clustering task, while choosing 2 or 8 dimensions yields degraded performance.

The conclusion of this section is that our spectral clustering of the MB connectome via $GMM \circ ASE$, with principled model selection for choosing embedding dimension and mixture complexity, yields meaningful results: a single Gaussian cluster for each of MBIN, MBON, and PN, and multiple clusters for KC. That is, we have one substantial revision to Figure 1’s illustration of the larval *Drosophila* mushroom body connectome as a directed graph on

four neuron types: significant substructure associated with the KC neurons. It is a more satisfactory model of this KC substructure that we pursue in the next section.

4 Semiparametric spectral modeling

The spectral clustering results of the previous section – a single Gaussian cluster for each of MBIN, MBON, and PN, and from at least 3 to as many as 8 Gaussian clusters for KC – hint at the possibility of a continuous, rather than discrete, structure for the KC.

Eichler et al. (2017) describes so-called “claws” associated with each KC neuron, and posits that KCs with only 1 claw are the oldest, followed in decreasing age by multi-claw KCs (from 2 to 6 claws), with finally the youngest KCs being those with 0 claws. Figure 7 and Table 7 use this additional neuronal information to show that the multiple clusters for the KC neurons are capturing neuron age – and in a seemingly coherent geometry.

As the clusters for the KC neurons are capturing neuron age – a continuous vertex attribute – in a seemingly coherent geometry, this section introduces the “latent structure model” (LSM) generalization of the SBM together with the principled semiparametric spectral modeling methodology $SemiparGMM \circ ASE$ associated thereto. Specifically, we fit a continuous curve to (the KC subset of) the data in latent space and show that traversal of this curve corresponds monotonically to neuron age.

We digress for a moment, to motivate our approach to the task at hand . . . and to develop, under the impetus of connectome modeling, a new direction for the theory & methods of statistical modeling for random graphs. (“The wealth of your practical experience with sane and interesting problems will give to mathematics a new direction and a new impetus.” – Leopold Kronecker to Hermann von Helmholtz (1888).)

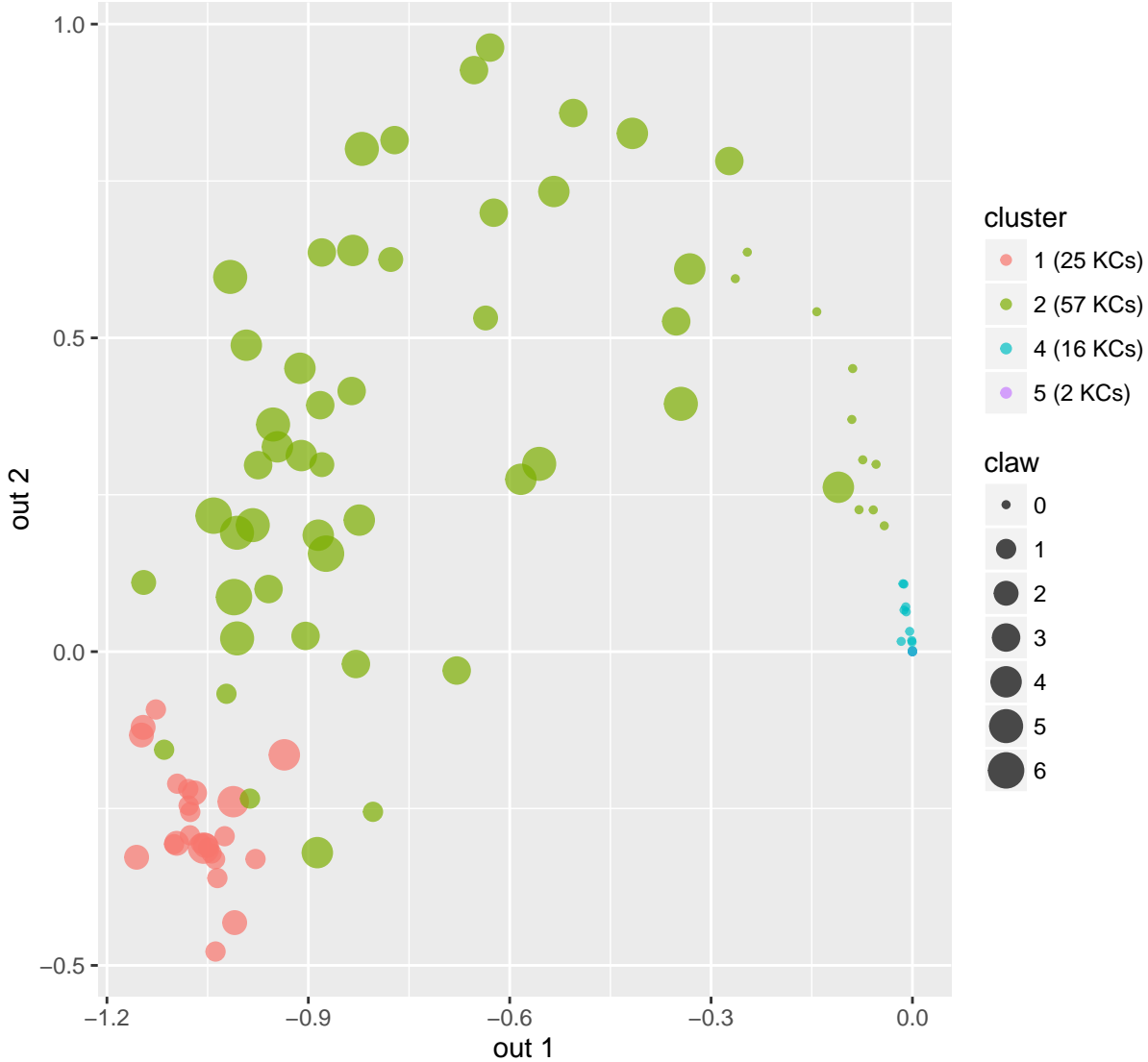


Figure 7: The multiple clusters for the KC neurons are capturing neuron age. Depicted are the first two dimensions for the KC neuron out-vectors, with color representing $\hat{K} = 6$ cluster membership – recall from Table 1 that the $n_{KC} = 100$ KCs are distributed across multiple clusters, with 25 neurons in cluster #1, 57 in #2, 0 in #3, 16 in #4, 2 in #5, and 0 in #6. The size of the dots represent the number of claws associated with the neurons. We see from the scatter plot that the embedded KC neurons arc from oldest (one-claw, lower left, cluster 1, in red), up and younger (more claws) through cluster 2 in green, and back down to youngest (zero-claw, clusters 4 & 5). See also Table 7. Recall that this is a two-dimensional visualization of six-dimensional structure.

cluster	1	2	3	4	5	6
#KCs	25	57	0	16	2	0
claw: 1 (oldest)	15	4	—	0	0	—
claw: 2	7	4	—	0	0	—
claw: 3	0	15	—	0	0	—
claw: 4	3	13	—	0	0	—
claw: 5	0	8	—	0	0	—
claw: 6	0	3	—	0	0	—
claw: 0 (youngest)	0	10	—	16	2	—

Table 7: The multiple clusters for the KC neurons are capturing neuron age via the number of claws associated with the neuron. We see from the $\widehat{K} = 6$ clustering table, for the $n_{KC} = 100$ KC neurons, that cluster 1 captures predominantly older neurons, cluster 2 captures both old and young neurons, and clusters 4 & 5 capture only the youngest neurons. See also Figure 7.

An alternative formulation for the directed SBM is as a latent position model (LPM) a la Hoff et al. (2002). Here one considers latent positions $X_i \sim^{iid} F$ on \mathbb{R}^d , and the graph is generated from the X_i via a link function or kernel (e.g. distance $d(\cdot, \cdot)$ or inner product $\langle \cdot, \cdot \rangle$). In particular, ASE – an SVD of the adjacency matrix – begs for an inner product kernel (that is, a random dot product graph, or RDPG; see e.g. Sussman et al. (2012)).

Definition 1 (Directed Random Dot Product Graph (RDPG)). Let $d_{out} = d_{in}$, and let F be a distribution on a set $\mathcal{X} = \mathcal{Y} \times \mathcal{Z} \subset \mathbb{R}^{d_{out}} \times \mathbb{R}^{d_{in}}$ such that $\langle y, z \rangle \in [0, 1]$ for all $y \in \mathcal{Y}$ and $z \in \mathcal{Z}$. We say that $(A, X) \sim \text{RDPG}(F)$ is an instance of a directed random dot product graph (RDPG) if $X = [(Y_1, Z_1), \dots, (Y_n, Z_n)]^\top$ with $(Y_i, Z_i) \stackrel{i.i.d.}{\sim} F$, and $A \in \{0, 1\}^{n \times n}$ is a hollow matrix satisfying

$$\mathbb{P}[A|X] = \prod_{i \neq j} (Y_i^\top Z_j)^{A_{ij}} (1 - Y_i^\top Z_j)^{1 - A_{ij}}.$$

The SBM as a latent position model says the latent position distribution F is mixture of point masses, with the block membership probability vector given by the weights on these point masses and, for the RDPG, the block connectivity probability matrix generated by their inner products.

Definition 2 (Directed Stochastic Block Model (SBM)). Let $d_{out} = d_{in}$, with $d = d_{out} + d_{in}$. We say that an n vertex graph $(A, X) \sim \text{RDPG}(F)$ is a directed stochastic block model (SBM) with K blocks if the distribution F is a mixture of K point masses,

$$dF = \sum_{k=1}^K \rho_k \delta_{x_k},$$

with block membership probability vector $\vec{\rho}$ in the unit $(K - 1)$ -simplex and distinct latent positions given by $x = [x_1, x_2, \dots, x_K]^\top \in \mathbb{R}^{K \times d}$. The first d_{out} elements of each latent position x_k are the out-vectors, denoted y_k , and the remaining d_{in} elements are the in-vectors z_k . We write $G \sim \text{SBM}(n, \vec{\rho}, yz^\top)$, and we refer to $yz^\top \in \mathbb{R}^{K, K}$ as the block connectivity probability matrix for the model.

The CLT for ASE of an SBM (Athreya et al., 2016) says that the \widehat{X}_i behave approximately as a random sample from a Gaussian mixture model (GMM) with the means and mixing coefficients of the mixture components providing a consistent estimate for F . (An analogous CLT for Laplacian spectral embedding is available in Tang and Priebe (2016).) In general, for an RDPG with any distribution F on \mathbb{R}^d such that inner products are in $[0, 1]$, the CLT yields approximate normality: $\widehat{X}_i | X_i = x_i \sim \varphi(x_i, \Sigma(x_i, F, n))$.

The above theoretical motivation is illustrated by considering the observed block connectivity probability matrix for our MB connectome data, under the assumption that it really is a 4-block directed SBM on the neuron types, given by

$$B_{observed} \approx \begin{bmatrix} 0.36 & 0.45 & 0.49 & 0 \\ 0.38 & 0 & 0.12 & 0 \\ 0 & 0.09 & 0.21 & 0 \\ 0.08 & 0 & 0 & 0 \end{bmatrix}.$$

The SVD of $B_{observed}$ provides four 4-dimensional in-vectors and four 4-dimensional out-vectors – the true latent positions for an SBM with block connectivity probability matrix $B_{observed}$. Together with the observed block membership probability vector $\rho_{observed} = [n_{KC}, n_{MBIN}, n_{MBON}, n_{PN}]/n = [100, 21, 29, 63]/213$, this yields a synthetic mushroom body directed SBM, dubbed “**synthMB**”, with latent positions $X_i \sim^{iid} F_{\text{synthMB}}$ where F_{synthMB} is the weighted mixture of four point masses in \mathbb{R}^8 . These four point masses are depicted in Figure 8 via brown concentric circles. ASE provides estimated latent positions \hat{X}_i for a large (10000-vertex) graph generated from **synthMB**; these are depicted in gold in Figure 8 and agree with the truth as large-sample approximation theory demands. ASE provides estimated latent positions \hat{X}_i for a small graph generated from **synthMB** with precisely $n = 213$ vertices in precisely their observed neuron type proportions; these are depicted in grey diamonds in Figure 8 and demonstrate that the large-sample approximation provides some practical guidance but has not entirely kicked in at $n = 213$. The colored circles in Figure 8 depict the actual MB connectome embedding of the four neuron types; one can see that the real embedded MBIN, MBON, and PN are behaving approximately as expected with respect to **synthMB** ... but clearly KC requires latent structure more complex than just **synthMB**’s point mass.

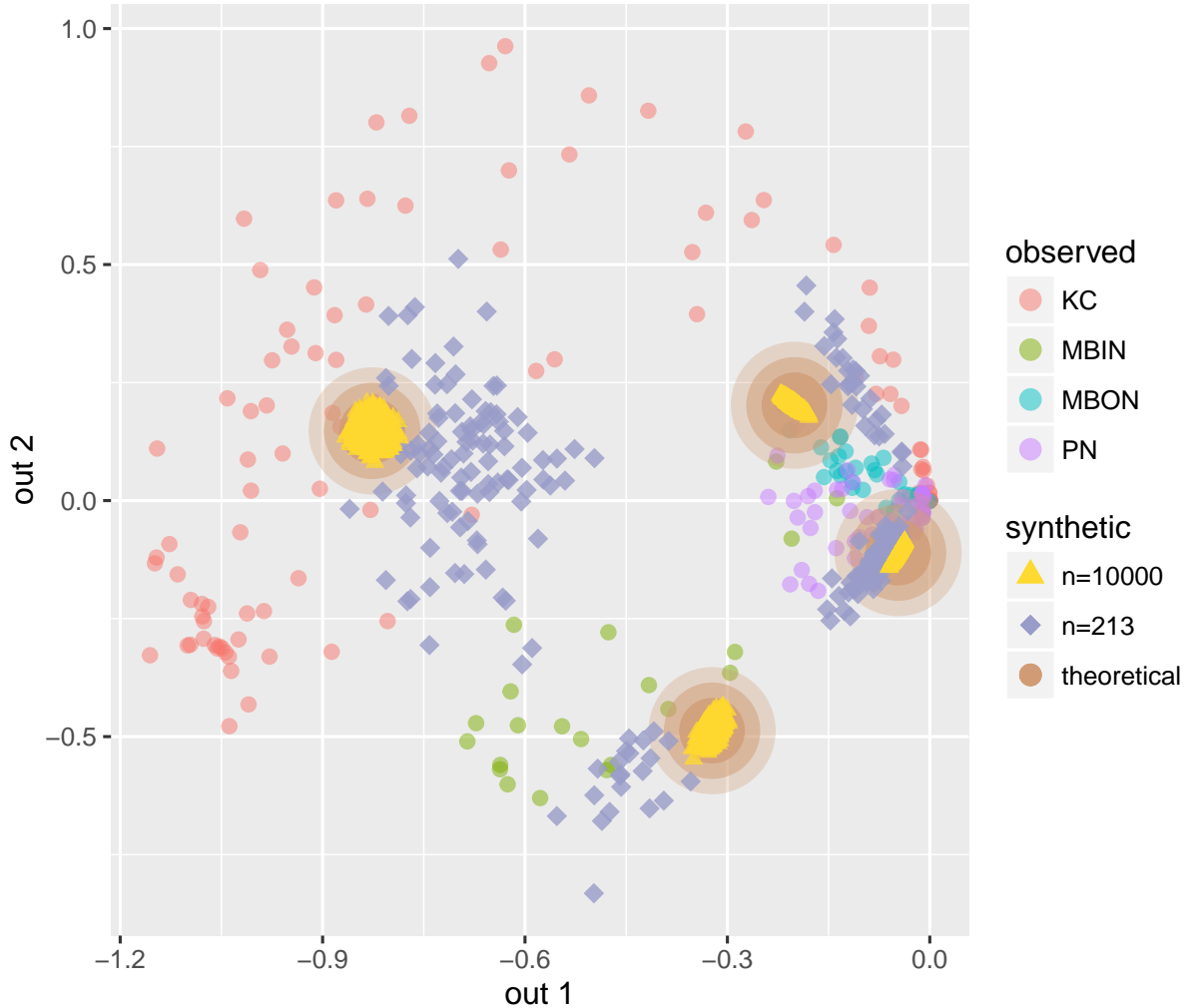


Figure 8: Illustrative spectral embedding results for synthetic mushroom body directed SBM (*synthMB*). For the observed MB connectome, the embedded MBIN, MBON, and PN are behaving as predicted, but clearly KC requires latent structure more complex than just *synthMB*'s point mass. Recall that this is a two-dimensional visualization of six-dimensional structure.

All models are wrong. We have demonstrated that the MB connectome is not a 4-block SBM, and this model's usefulness has been in allowing us to identify a first-order sense in which the real data deviate from the model. The $GMM \circ ASE$ results of a single cluster for each of MBIN, MBON, and PN, and multiple clusters indicating a geometrically coherent structure

for KC compel us to use, as our new model, a generalization of SBM allowing KC a *curve*, rather than just a point, in latent space. We now endeavor to model the MB connectome as a 4 component latent structure model (LSM), where LSM denotes the “generalized SBM” where each “block” may be generalized from point mass latent position distribution to latent position distribution with support on some curve (with the "block" curves disconnected, as (of course) are SBM’s point masses). So LSM does have structure ... just not quite so simple as SBM; and LSM will exhibit clustering ... just not quite so simple as SBM. Thanks to the foregoing RDPG discussion, we see that the LSM is easily formulated by considering latent position distribution F more general than SBM’s finite mixture of point masses but not arbitrary as for the fully general RDPG.

Definition 3 (Directed Latent Structure Model (LSM)). Let $d_{out} = d_{in}$, and let F be a distribution on a set $\mathcal{X} = \mathcal{Y} \times \mathcal{Z} \subset \mathbb{R}^{d_{out}} \times \mathbb{R}^{d_{in}}$ such that $\langle y, z \rangle \in [0, 1]$ for all $y \in \mathcal{Y}$ and $z \in \mathcal{Z}$. We say that an n vertex graph $(A, X) \sim \text{RDPG}(F)$ is a directed latent structure model (LSM) with K “structure components” if the support of distribution F is a mixture of K (disjoint) curves,

$$dF = \sum_{k=1}^K \rho_k dF_k(x),$$

with block membership probability vector $\vec{\rho}$ in the unit $(K - 1)$ -simplex and F_k supported on \mathcal{C}_k and $\mathcal{C}_1, \dots, \mathcal{C}_K$ disjoint. We write $G \sim \text{LSM}(n, \vec{\rho}, (F_1, \dots, F_K))$.

NB: The degree-corrected SBM (Karrer and Newman, 2011) is a special case of LSM where each \mathcal{C}_k is a *ray*.

NB: The “hierarchical stochastic block model” (HSBM), introduced and exploited in Lyzinski et al. (2017), is a similarly “generalized SBM” where each “block” may be generalized from point mass latent position distribution to structured latent position distribution with support given by a hierarchical mixture of points.

So now we investigate our MB connectome as an LSM with latent positions $X_i \sim^{iid} F$ where F is no longer a mixture of four point masses with one point mass per neuron type but instead $\text{support}(F)$ is three points and a continuous curve \mathcal{C}_{KC} .

The approximate normality provided by the CLT for ASE of an RDPG compels us to consider estimating F via a semiparametric Gaussian mixture model for the \widehat{X}_i 's. Let H be a probability measure on a parameter space $\Theta \subset \mathbb{R}^d \times S_{d \times d}$, where $S_{d \times d}$ is the space of d -dimensional covariance matrices, and let $\{\varphi(\cdot; \theta) : \theta \in \Theta\}$ be a family of normal densities. Then the function given by

$$\alpha(\cdot; H) = \int_{\Theta} \varphi(\cdot; \theta) dH(\theta)$$

is a semiparametric GMM. $H \in \mathcal{M}$ is referred to as the mixing distribution of the mixture, where \mathcal{M} is the class of all probability measures on Θ . If H consists of a finite number of atoms, then $\alpha(\cdot; H)$ is a finite normal mixture model with means, variances and proportions determined by the locations and weights of the point masses. Lindsay (1983) provides theory for maximum likelihood estimation (MLE) in the semiparametric GMM.

Thus (ignoring covariances for presentation simplicity, so that $\theta \in \mathbb{R}^d$ is the component mean vector) we see that the ASE RDPG CLT suggests estimating the probability density function of the embedded MB connectome $\widehat{X}_1, \dots, \widehat{X}_{n=213}$, under the LSM assumption, as the semiparametric GMM $\alpha(\cdot; H)$ with $\Theta = \mathbb{R}^{\widehat{d}=6}$ and where $H = F$ is supported by three points and a continuous curve \mathcal{C}_{KC} . Note that in the general case, where Θ includes both means and covariance matrices, we have $H = H_{F,n}$. However, we emphasize that it is F (or dF) that is the ‘‘connectome code’’ – the key to the generative model; the covariances (in dH but not in dF) that we are ‘‘ignoring for presentation simplicity’’ are in fact nuisance parameters from the perspective of the connectome code. The ASE RDPG CLT provides a large-sample approximation for $H_{F,n}$, and provides a mean-covariance constraint so that if we knew the latent position distribution F we would have no extra degrees of freedom (though perhaps a more challenging MLE optimization problem). As it is, we do our fitting in the general case, with simplifying constraints on the covariance structure associated with \mathcal{C}_{KC} .

The MLE (continuing to ignore covariances) is given by

$$d\widehat{H}(\theta) = \sum_{k=1}^3 \widehat{\rho}_k I\{\theta = \widehat{\theta}_k\} + \left(1 - \sum_{k=1}^3 \widehat{\rho}_k\right) \widehat{\rho}_{KC}(\theta) I\{\theta \in \widehat{\mathcal{C}}_{KC}\}$$

where $\hat{\theta}_1, \hat{\theta}_2, \hat{\theta}_3$ are given by the means of the $GMM \circ ASE$ Gaussian mixture components for MBIN, MBON, and PN, and $\hat{\mathcal{C}}_{KC} \subset \mathbb{R}^d$ is a one-dimensional curve. Figure 9 displays the MLE results from an EM optimization for the curve $\hat{\mathcal{C}}_{KC}$ constrained to be quadratic, as detailed in the Appendix. (Model testing for \mathcal{C}_{KC} in \mathbb{R}^6 does yield quadratic: testing the null hypothesis of linear against the alternative of quadratic yields clear rejection ($p < 0.001$), while there is insufficient evidence to favor H_A cubic over H_0 quadratic ($p \approx 0.1$.)

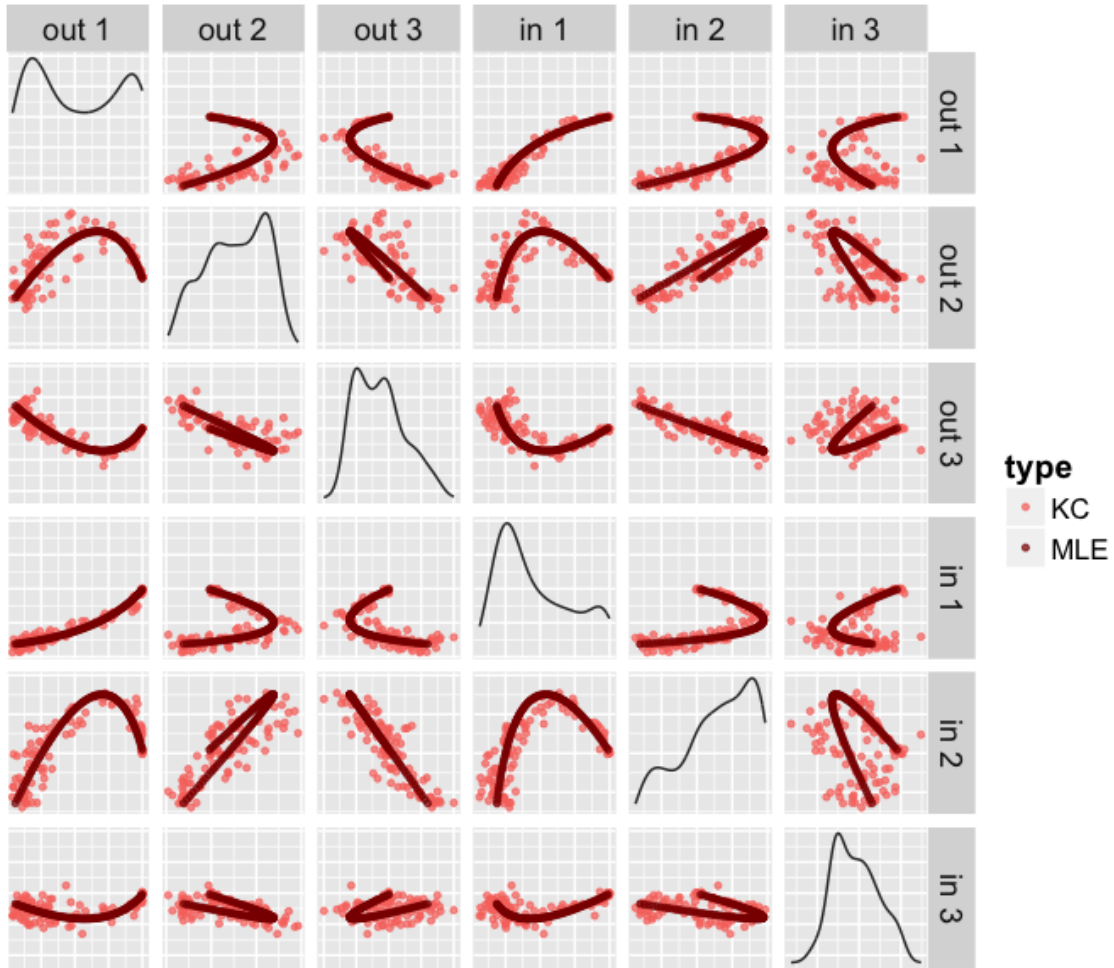


Figure 9: Semiparametric MLE $\hat{\mathcal{C}}_{KC}$ for the KC latent-space curve in \mathbb{R}^6 .

That is, (continuing to ignore covariances) our structure discovery via $SemiparGMM \circ ASE$ yields an \mathbb{R}^6 latent position estimate for the MB connectome – a *connectome code* for the

larval *Drosophila* mushroom body – as a semiparametric Gaussian mixture of three point masses and a continuous parameterized curve $\hat{\mathcal{C}}_{KC}$; the three Gaussians correspond to three of the four neuron types, and the curve corresponds to the fourth neuron type (KC) with the parameterization capturing neuron age. See Figure 10.

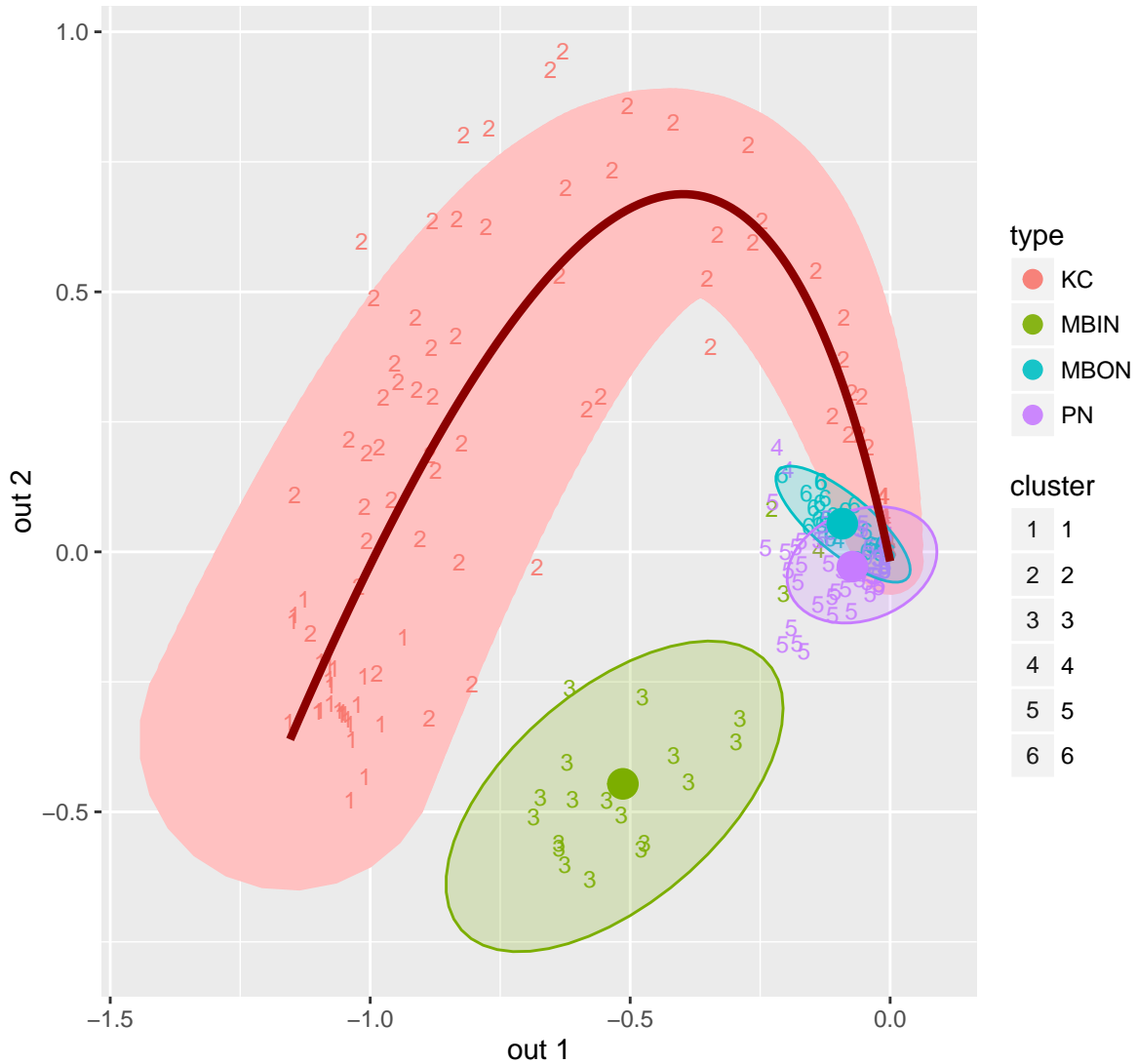


Figure 10: Semiparametric spectral latent space estimate of our MB connectome as three Gaussians and a KC curve: colors distinguish the four neuron types and numbers distinguish the original $\hat{K} = 6$ clusters. Recall that this is a two-dimensional visualization of six-dimensional structure.

Eichler et al. (2017) suggests distance-to-neuropile δ_i – the distance to the MB neuropile from the bundle entry point of each KC neuron i – as a proxy for neuron age, and analyzes this distance in terms of number of claws for neuron i . See Figure 11. We now demonstrate that the correlation of this distance with the KC neurons’ projection onto the parameterized curve $\hat{\mathcal{C}}_{KC}$ is highly significant – this semiparametric spectral model captures neuroscientifically important structure in the connectome. To wit, we project each KC neuron’s embedding onto our parameterized $\hat{\mathcal{C}}_{KC}$ and study the relationship between the projection’s position on the curve, t_i , and the neuron’s age through the distance proxy δ_i . See Figures 12 and 13. We find significant correlation of δ_i with t_i – Spearman’s $s = -0.271$, Kendall’s $\tau = -0.205$, Pearson’s $\rho = -0.304$, with $p < 0.01$ in each case – demonstrating that our semiparametric spectral modeling captures biologically relevant neuronal properties.

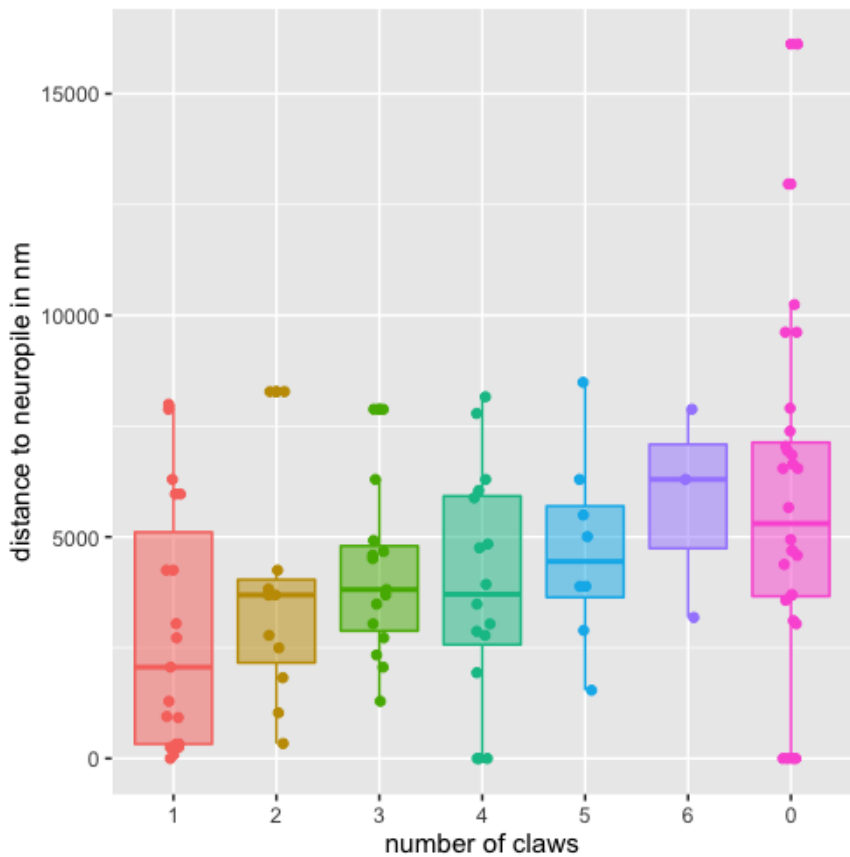


Figure 11: Relationship between number of claws and distance δ_i (a proxy for age) for the KC neurons, from Eichler et al. (2017).

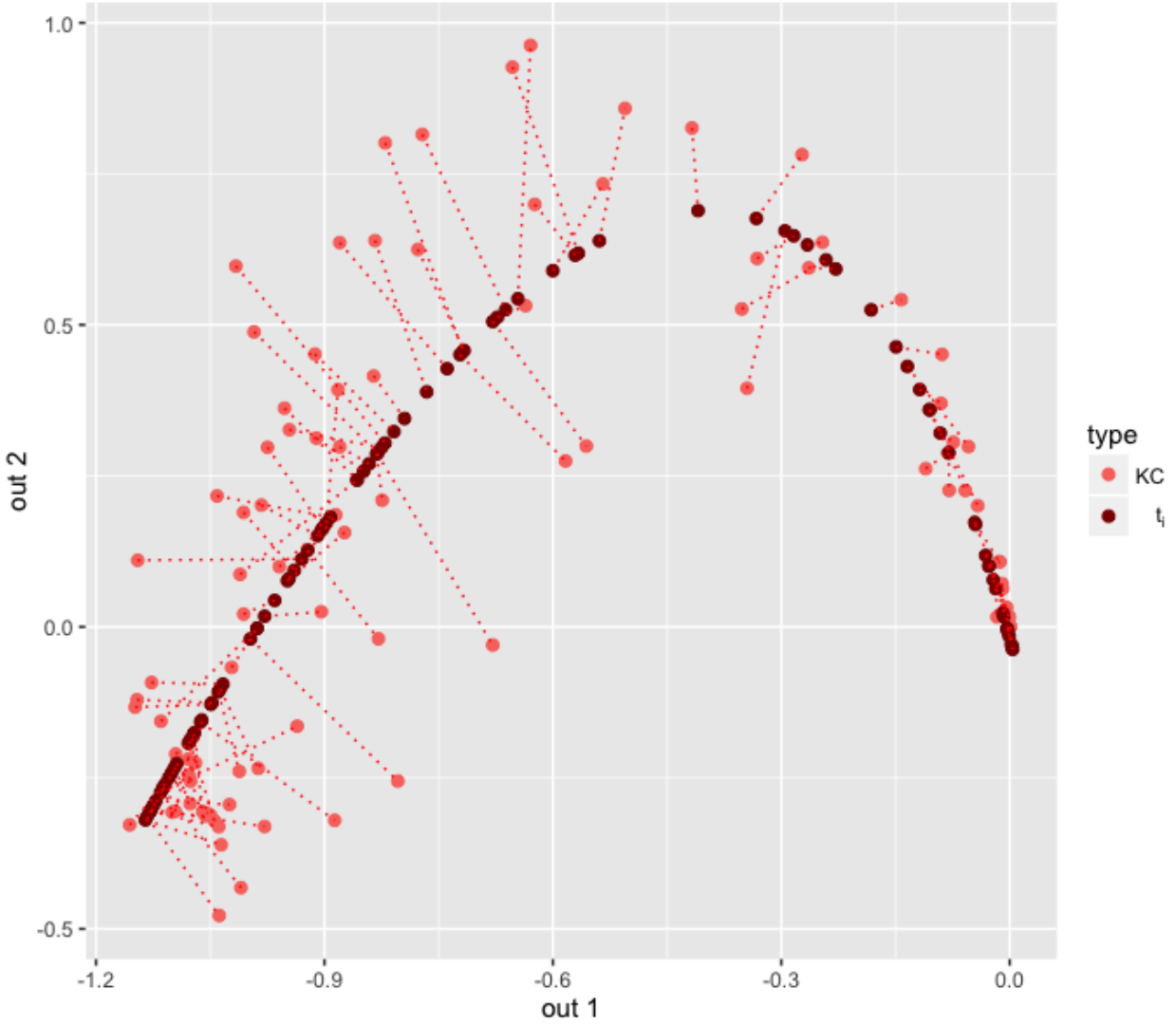


Figure 12: Projection of KC neurons onto the quadratic curve $\widehat{\mathcal{C}}_{KC}$, yielding projection point t_i for each neuron. Recall that this is a two-dimensional visualization of six-dimensional structure.

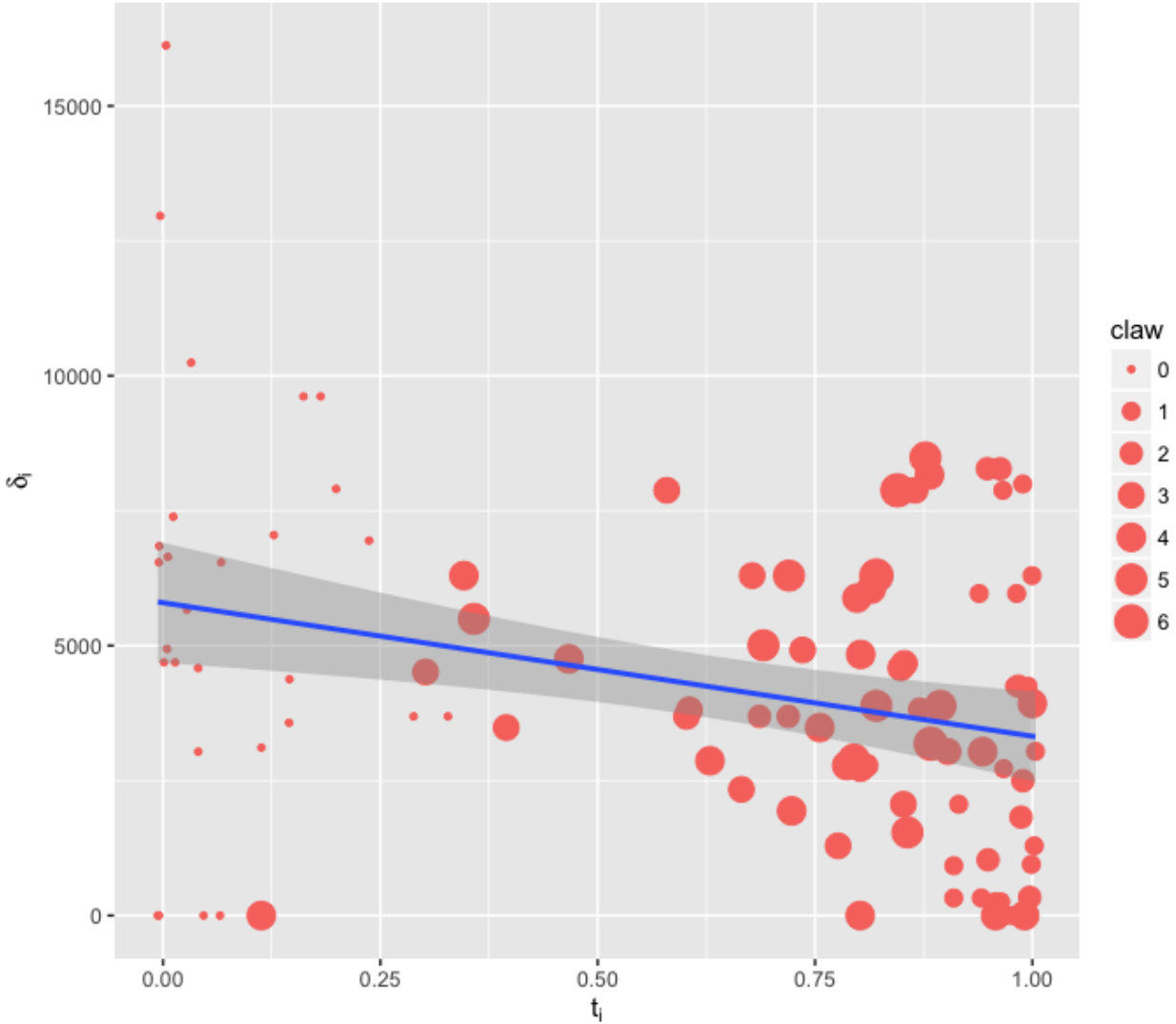


Figure 13: The correlation between the projection points t_i on the quadratic curve \widehat{C}_{KC} and distance δ_i (a proxy for age) for the KC neurons is highly significant, demonstrating that our semiparametric spectral modeling captures biologically relevant neuronal properties.

5 Discussion

We briefly discuss a few of the many issues raised by this investigation: first a few points of neuroscientific relevance, and then some technical points regarding our methodology.

5.1 Neuroscientific discussion points

5.1.1 Directed! Weighted?

Inspection of the six-dimensional embedding of our MB connectome (Figure 3) suggests that neither the in-vectors nor the out-vectors alone suffice. Figure 14 left panel demonstrates this quantitatively.

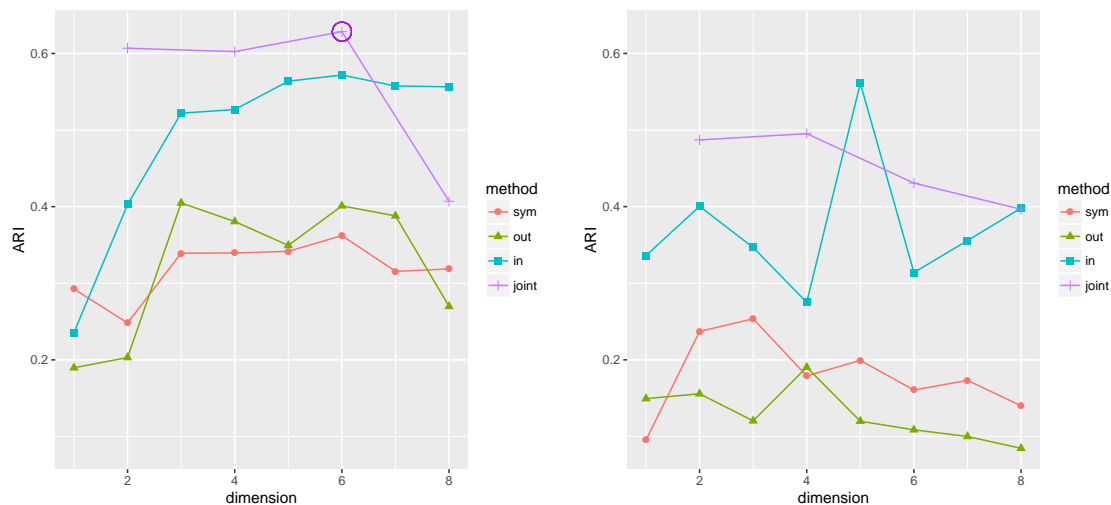


Figure 14: Left panel: Directed! Plotting ARI vs. dimension for the $GMM \circ ASE$ analysis of the MB connectome demonstrates that using both in- and out-vectors is superior to using in-only, using out-only, or considering a symmetrized adjacency matrix. That is, the directed nature of this connectome is essential to our analysis.

Right panel: Weighted? Plotting ARI vs. dimension for the $GMM \circ ASE$ analysis of the *weighted* MB connectome demonstrates, in comparison with Figure 14, that the best weighted version yields inferior results. (Transformation of the weights can make the weighted results competitive.)

The connectome is a multi-graph – there are multiple edges (synapses) between neurons. We have analyzed the unweighted version. ASE is applicable to weighted graphs, and the analogous $GMM \circ ASE$ analysis with the weighted MB connectome yields inferior results – see Figure 14 right panel. NB: It does appear that one might do better using some

transformation of the weights – e.g., $w' = \log(1 + w)$; this is an area of current investigation.

5.1.2 Synthetic validation

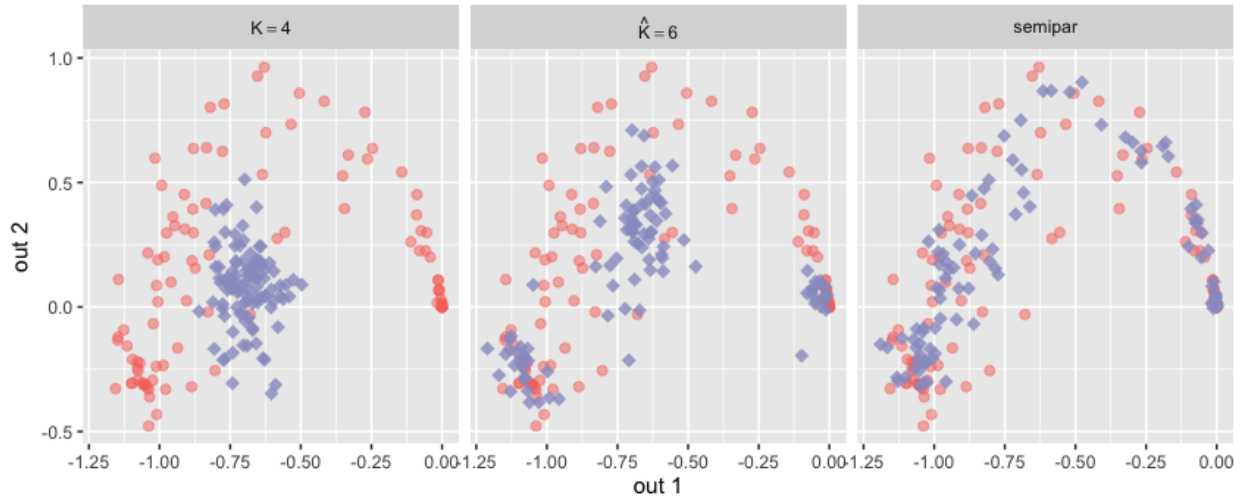


Figure 15: Three synthetic KC sampling schemes, with sampled points depicted as grey diamonds and true KC embeddings depicted as red circles. Left: the $K = 4$ **synthMB** SBM from Section 4. Center: the $\hat{K} = 6$ $GMM \circ ASE$ SBM from Section 3. Right: the $SemiparGMM \circ ASE$ estimate obtained under the LSM model from Section 4. Recall that these are two-dimensional visualizations of six-dimensional structure.

Figure 15 presents synthetic KC sampling (grey diamonds) vs. true KC embedding (red circles). The left panel shows the **synthMB** sampling from Section 4 – just the KCs from Figure 8; sampling from the $K = 4$ SBM, which models KC with a single latent space Gaussian, demonstrates the need for a more elaborate KC model. The center panel shows the synthetic sampling using the best estimate obtained via $GMM \circ ASE$ in Section 3; sampling from the $\hat{K} = 6$ SBM, which models KC with three latent space Gaussians, demonstrates superiority over **synthMB** but still the need for a more elaborate KC model. The right panel shows the synthetic sampling using the best estimate obtained via the $SemiparGMM \circ ASE$ methodology developed in Section 4; here we see that sampling from the structured LSM,

which models KC with a semiparametric GMM in latent space, reproduces the KC structure amazingly well.

5.1.3 Outlier detection and characterization

Our semiparametric connectome code greatly facilitates the search for and characterization of outliers. For example, there is one outlier readily apparent in Figure 13 – a KC neuron at the bottom left with small t_i , $\delta_i = 0$, and four claws. (This is the larger green dot at $\approx (-0.1, 0.25)$ in Figure 7, perhaps but not quantitatively an outlier without our parameterized semiparametric curve \widehat{C}_{KC} ; nothing stands out too dramatically in the four-claw boxplot in Figure 11.) Neuroscientifically, post facto investigation shows that this neuron is clearly an outlier in the group of mature KCs, unusual in that it has many synapses in the calyx but isn't fully grown out yet in the lobes, explaining why this neuron might group with the 0 claw KCs having small t_i in Figure 13.

This result serves as both an example of the utility of our theory and methods for subsequent neuroscientific investigations and an empirical validation of our claim that the LSM and the associated *SemiparGMM* \circ *ASE* estimation methodology capture biologically relevant neuronal properties in the MB connectome.

5.1.4 Hemispheric validation: right vs. left

We have considered the right hemisphere MB. In the absence of $m > 1$ – that is, MB connectomes for other larval *Drosophila* animals, which data are not yet available – we compare and contrast our estimate obtained on the right connectome with data from the left connectome. (Indeed, we developed the theory & methods and the *SemiparGMM* \circ *ASE* estimate for the right hemisphere MB without ever looking at the left hemisphere MB data ... for just this validation purpose.) Figure 16 shows that the *SemiparGMM* \circ *ASE* right hemisphere MB estimate (right panel – a repeat of Figure 10) not only captures the structure in the right connectome, but also provides compelling evidence (left panel) that the same

right connectome estimate captures the structure in the left connectome data as well. (NB: The analogous result holds when we estimate using the left connectome – the left estimate captures the right structure.)

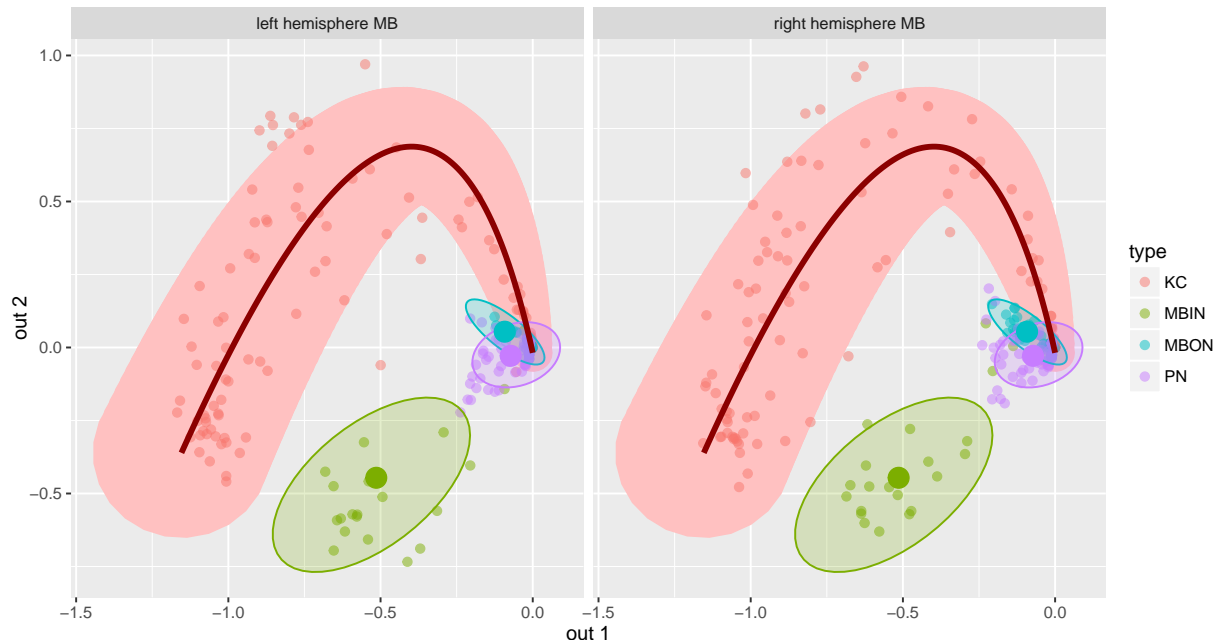


Figure 16: Right: the right hemisphere MB data and $SemiparGMM \circ ASE$ estimate; the structure is captured. Left: the left hemisphere MB data superimposed on the right hemisphere MB estimate; the fit is compelling. Recall that these are two-dimensional visualizations of six-dimensional structure.

5.2 Methodological discussion points

Our work is similar in spirit to the pioneering “color circle” perception work of Ekman (1954), the “horseshoes” structure discovery of Diaconis et al. (2008), etc.

It is established (Tang and Priebe, 2016) that there is no uniformly best choice between adjacency spectral embedding (ASE) and Laplacian spectral embedding (LSE) for spectral clustering. The extension of ASE to directed graphs is straightforward (as we have seen), while LSE for directed graphs remains an open area of investigation (see, e.g., Section 4.3.2

in the recent survey by Malliaros and Vazirgiannis (2013)).

It is established (Tang and Priebe, 2016) that K -means is inferior to GMM for spectral clustering. That is, however, a limit theorem; it says little about our real MB connectome with $n = 213$ vertices. Therefore, we did consider replacing GMM with K -means in the Section 3 investigation, everything else remaining the same; the results were that we did still get $\hat{K} = 6$, but the clustering solution was evidently much less consistent with the true neuron types, and ARI was significantly degraded (0.42 with K -means vs. 0.63 with GMM).

In practice, for small n , it is empirically useful to augment the diagonal of the adjacency matrix (default: $degree(v)/(n - 1)$ for undirected graphs) prior to ASE. As a general rule, we use this augmentation. For thoroughness, we did consider $GMM \circ ASE$ without diagonal augmentation; the results were that we did still get $\hat{d} = 6$, but the clustering solution was evidently much less consistent with the true neuron types, and ARI was significantly degraded (0.36 without diagonal augmentation vs. 0.63 with).

6 Conclusion

In a recent PNAS opinion piece (Geman and Geman, 2016), Donald & Stuart Geman describe the ‘usual explanation’ for a perceived lack of ‘fundamental innovation’ in areas such as brain science: that such systems are somehow ‘inherently too complex,’ ‘unsimplifiable,’ ‘not amenable to abstraction.’ The quest for a connectome code that reveals the principles and mechanisms of the connectivity of neural circuits seems to be in keeping with their position that this ‘usual explanation’ may be shortsighted.

Motivated by the results of a spectral clustering investigation of the recently-reconstructed synapse-level larval *Drosophila* mushroom body structural connectome, which demonstrate conclusively that modeling the Kenyon Cells (KC) demands additional latent space structure, we have developed semiparametric spectral modeling. Exploratory data analysis suggests that the MB connectome can be productively approximated by a 4 component latent structure model (LSM), and the resulting MB connectome code derived via $SemiparGMM \circ ASE$

captures biologically relevant neuronal properties.

Of course, the true connectome code is more elaborate, and cannot be completely encompassed by any simple latent position model – such a model precludes the propensity for transitivity, e.g. – but our semiparametric spectral modeling provides another step along the path. In terms of a (partial) ladder of biological scales – e.g., *C. elegans*, *Drosophila*, zebrafish, mouse, primate, and humans – this work moves us off the first rung for analysis of a complete neurons-as-vertices and synapses-as-edges connectome.

Next steps include extending this investigation to (currently unavailable) data for (a) new complete synapse-level larval *Drosophila* MB structural connectomes from different animals, (b) new complete supersets of the synapse-level larval *Drosophila* MB structural connectome, and (c) new complete synapse-level structural connectomes from different species, such as the adult *Drosophila*. Furthermore, multi-modal connectome analyses, combining complete synapse-level structural connectomes with other modalities such as behavioral connectomes obtained via optogenetics and activity-based connectomes obtained via calcium imaging, promise additional advances in connectome coding.

Appendix: Constrained Maximum Likelihood Estimation of the Semiparametric Gaussian Mixture Model for Adjacency Spectral Embedding of a Latent Structure Model

The CLT for the ASE of an RDGP (Athreya et al., 2016) gives that the $\hat{X}_1, \dots, \hat{X}_n$ are approximately normal about the true (unobserved) latent positions X_1, \dots, X_n . Of course, this is a large-sample (asymptotic) result; furthermore, the theory does *not* provide mutual independence of all n embedded points, but rather of only a fixed finite n' of the $\hat{X}_1, \dots, \hat{X}_n$, as $n \rightarrow \infty$. Nevertheless, we proceed assuming independence with what we call “MLE in the embedding space”.

We model the MB connectome embedding $\widehat{X}_1, \dots, \widehat{X}_n \in \mathbb{R}^d$ as a semiparametric GMM

$$\alpha(\cdot; H) = \int_{\Theta} \varphi(\cdot; \theta) dH(\theta)$$

where $\{\varphi(\cdot; \theta) : \theta \in \Theta\}$ is the family of d -dimensional Gaussian densities, with $\theta = (\mu, \Sigma)$, $\mu \in \mathbb{R}^d$ and $\Sigma \in S_{d \times d}$; H represents a probability measure on the parameter space $\Theta \subset \mathbb{R}^d \times S_{d \times d}$.

Our exploratory data analysis presented above suggests we consider dH to be a four component mixture model, with the first three components being point masses and a final component (for the KC neurons) having continuous support on a one-dimensional curve \mathcal{C}_{KC} :

$$dH(\mu, \Sigma) = \sum_{k=1}^3 \rho_k I\{\mu = \mu_k, \Sigma = \Sigma_k\} + \left(1 - \sum_{k=1}^3 \rho_k\right) \rho_{KC}(\mu, \Sigma) I\{(\mu, \Sigma) \in \mathcal{C}_{KC}\}$$

where $\int_{\mathcal{C}_{KC}} \rho_{KC}(\mu, \Sigma) = 1$ and \mathcal{C}_{KC} is a curve in $\mathbb{R}^d \times S_{d \times d}$. (Note that the ASE CLT provides a mean-variance constraint which we do not attempt to take advantage of here.)

For the remainder of this appendix we focus on the final non-trivial component in dH , and consider

$$dH = \rho_{KC}(\mu, \Sigma) I\{(\mu, \Sigma) \in \mathcal{C}_{KC}\}$$

and the semiparametric MLE

$$\widehat{H} = \arg \max_{H \in \mathcal{M}} \sum_{i=1}^n \log \alpha(\widehat{X}_i; H)$$

over a space of constrained probability measures \mathcal{M} described below.

This optimization for \widehat{H} has been widely studied. Kiefer and Wolfowitz (1956) first established the consistency of the semiparametric MLE under suitable conditions. However, many issues remained unresolved until Laird (1978) and Lindsay (1983). The work of Lindsay (1983) has established that there indeed exists a maximizer \widehat{H} and provides conditions under which its uniqueness can be established; the nature of the maximizer \widehat{H} is further revealed to be that of a discrete distribution with finitely many mass points. Moreover Lindsay (1983) shows that the number of mass points K (which is random, depending upon the sample

$\widehat{X}_1, \dots, \widehat{X}_n$) is bounded above by the number of distinct observations in the sample; that is, $1 \leq K(\widehat{X}_1, \dots, \widehat{X}_n) \leq n$. These results indicate that simply applying the EM algorithm will serve the purpose of estimating H because the maximizer \widehat{H} is essentially a finite GMM. (Due to the limitations of the EM algorithm, the computational speed for such an estimation can be a challenge. Alternative computational approaches include Intra Simplex Direction Method (ISDM) by Lesperance and Kalbfleisch (1992), Generalized ISDM by Susko et al. (1998), and Constrained Newton Method (CNM) by Wang (2010). For a comprehensive review of semiparametric MLE for mixture models, see Lindsay and Lesperance (1995).)

Based on these previous results, and after settling on a value for K , we can directly fit a K -component Gaussian mixture to the data. To facilitate such an estimation and reduce the complexity of the optimization, *and motivated by the MB connectome exploratory data analysis presented in the main body of this paper*, we further assume that H is supported on

$$\begin{aligned} \mathcal{C}_{KC} = \{(\mu(t), \Sigma(t)) : & \mu(t) = (1-t)^2 m_1 + 2t(1-t)m_2 + t^2 m_3, \\ & \Sigma(t) = ((1-t)\sigma_1^2 + t\sigma_2^2)I_{d \times d}, \\ & 0 \leq t \leq 1\} \end{aligned}$$

where $m_1, m_2, m_3 \in \mathbb{R}^d$, $\sigma_1^2, \sigma_2^2 \in \mathbb{R}^+$ and $I_{d \times d}$ is the identity matrix. For $0 \leq t \leq 1$, $\mu(t)$ represents a quadratic curve in \mathbb{R}^d and $\Sigma(t)$ represents a linear structure for the covariance; thus, \mathcal{C}_{KC} is a curve in $\mathbb{R}^d \times S_{d \times d}$. This parametrization has significantly simplified the structure of H . Therefore, after settling on $K = 7$ for the KC neurons based on a BIC analysis analogous to that presented in Figure 6 but accounting for our semiparametric constraints, we fit the following K -component GMM to the data:

$$g(\cdot) = \sum_{j=1}^K \pi_j \varphi(\cdot; \mu_j, \Sigma_j),$$

where (μ_j, Σ_j) are equally spaced on the curve \mathcal{C}_{KC} . Since such a Gaussian mixture restricts its means and variances to satisfy the support of H , the estimation can be easily performed using the EM algorithm.

We propose the following EM algorithm to estimate such a mixture model.

1. Given initial values: $\{m_1, m_2, m_3 \in \mathbb{R}^d, \sigma_1^2, \sigma_2^2 \in \mathbb{R}^+, \pi \in \mathbb{R}^K\}$.
2. E step: compute the conditional expectation of class labels

$$z_{ij} = \frac{\pi_j \varphi(x_i, \mu_j, \Sigma_j)}{\sum_{j=1}^K \pi_j \varphi(x_i, \mu_j, \Sigma_j)}$$

where $(\mu_j, \Sigma_j) \in \mathcal{C}_{KC}$.

3. M step: maximize the complete likelihood $\mathcal{L}^c = \sum_{i=1}^n \sum_{j=1}^K z_{ij} \log(\pi_j \varphi(x_i, \mu_j, \Sigma_j))$ and obtain the parameter estimates

$$\hat{\pi}_j = \frac{1}{n} \sum_{i=1}^n z_{ij} \quad \text{and} \quad \{\hat{m}_1, \hat{m}_2, \hat{m}_3, \hat{\sigma}_1^2, \hat{\sigma}_2^2\} = \arg \max_{m_1, m_2, m_3, \sigma_1^2, \sigma_2^2} \mathcal{L}^c$$

such that $\mu_j = \mu((j-1)/(K-1))$ and $\Sigma_j = \Sigma((j-1)/(K-1))$ for $j = 1, \dots, K$.

4. Use the estimates from Step 3 as the initial values, and repeat Steps 2 and 3 until convergence.
5. Let

$$\begin{aligned} \widehat{\mathcal{C}}_{KC} &= \{(\mu(t), \Sigma(t)) : \mu(t) = (1-t)^2 \hat{m}_1 + 2t(1-t) \hat{m}_2 + t^2 \hat{m}_3, \\ &\quad \Sigma(t) = ((1-t) \hat{\sigma}_1^2 + t \hat{\sigma}_2^2) I_{d \times d}, \\ &\quad 0 \leq t \leq 1\}, \\ \hat{\rho}(\mu(t), \Sigma(t)) &= \sum_{j=1}^K \pi_j I\{\mu(t) = \hat{\mu}_j, \Sigma(t) = \hat{\Sigma}_j\}. \end{aligned}$$

We apply the proposed EM algorithm on the adjacency spectral embeddings of $n = 100$ KC neurons. The results are presented in Figure 9 in the manuscript, where the bold curve represents $\widehat{\mathcal{C}}_{KC}$.

Kiefer and Wolfowitz (1956) established the consistency of the semiparametric MLE \hat{H} . Since our estimation is conducted in a restricted parameter space \mathcal{C}_{KC} , as long as the true parameter is inside this restricted parameter space the consistency of our estimator follows immediately:

Corollary 4. *Suppose the true probability measure H is supported on \mathcal{C}_{KC} . As $n \rightarrow \infty$, $\hat{m}_j \xrightarrow{P} m_j$ and $\hat{\sigma}_j^2 \xrightarrow{P} \sigma_j^2$; consequently, $I\{\theta \in \hat{\mathcal{C}}_{KC}\} \xrightarrow{P} I\{\theta \in \mathcal{C}_{KC}\}$.*

Acknowledgments

This work was partially supported by NSF BRAIN EAGER award DBI-1451081, DARPA XDATA contract FA8750-12-2-0303, DARPA SIMPLEX contract N66001-15-C-4041, and HHMI Janelia. The authors thank the Isaac Newton Institute for Mathematical Sciences, Cambridge, UK, for support and hospitality during the programme Theoretical Foundations for Statistical Network Analysis (EPSRC grant no. EP/K032208/1) where a portion of the work on this paper was undertaken. The authors thank Keith Levin and Joshua Cape for helpful comments and criticism.

References

- Akaike, H. (1974). A new look at the statistical model identification. *IEEE Transactions on Automatic Control* 19(6), 716–723.
- Athreya, A., C. E. Priebe, M. Tang, V. Lyzinski, D. J. Marchette, and D. L. Sussman (2016). A limit theorem for scaled eigenvectors of random dot product graphs. *Sankhya A* 78(1), 1–18.
- Bickel, P. J. and K. A. Doksum (2007). *Mathematical Statistics: Basic Ideas and Selected Topics* (2nd ed.), Volume 1 of *Holden-Day series in probability and statistics*. Prentice Hall.
- Chatterjee, S. (2015). Matrix estimation by universal singular value thresholding. *The Annals of Statistics* 43(1), 177–214.
- Chen, L., J. T. Vogelstein, V. Lyzinski, and C. E. Priebe (2016). A joint graph inference case study: the *C. elegans* chemical and electrical connectomes. *Worm* 5(2), e1142041.

- Danon, L., A. Díaz-Guilera, J. Duch, and A. Arena (2005). Comparing community structure identification. *Journal of Statistical Mechanics: Theory and Experiment* 2005(09), P09008.
- Diaconis, P., S. Goel, and S. Holmes (2008). Horseshoes in multidimensional scaling and local kernel methods. *The Annals of Applied Statistics* 2(3), 777–807.
- Eichler, K., F. Li, A. L. Kumar, Y. Park, I. Andrade, C. Schneider-Mizell, T. Saumweber, A. Huser, D. Bonnery, B. Gerber, R. D. Fetter, J. W. Truman, C. E. Priebe, L. F. Abbott, A. Thum, M. Zlatic, and A. Cardona (2017). The complete wiring diagram of a high-order learning and memory center, the insect mushroom body. *Nature*, accepted for publication.
- Ekman, G. (1954). Dimensions of Color Vision. *Journal of Psychology* 38, 467–474.
- Fishkind, D. E., D. L. Sussman, M. Tang, J. T. Vogelstein, and C. E. Priebe (2013). Consistent adjacency-spectral partitioning for the stochastic block model when the model parameters are unknown. *SIAM Journal on Matrix Analysis and Applications* 34, 23–39.
- Fraley, C. and A. E. Raftery (2002). Model-based clustering, discriminant analysis and density estimation. *Journal of the American Statistical Association* 97, 611–631.
- Geman, D. and S. Geman (2016). Opinion: Science in the age of selfies. *Proceedings of the National Academy of Sciences* 113(34), 9384–9387.
- Glasser, M. F., T. S. Coalson, E. C. Robinson, C. D. Hacker, J. Harwell, E. Yacoub, K. Ugurbil, J. Andersson, C. F. Beckmann, M. Jenkinson, S. M. Smith, and D. C. Van Essen (2016). A multi-modal parcellation of human cerebral cortex. *Nature* 536(7615), 171–178.
- Hagmann, P. (2005). *From diffusion MRI to brain connectomics*. Ph. D. thesis, STI, Lausanne.
- Hoff, P. D., A. E. Raftery, and M. S. Handcock (2002). Latent space approaches to social network analysis. *Journal of the American Statistical Association* 97(460), 1090–1098.

- Holland, P. W., K. B. Laskey, and S. Leinhardt (1983). Stochastic blockmodels: First steps. *Social networks* 5(2), 109–137.
- Hubert, L. and P. Arabie (1985). Comparing partitions. *Journal of Classification* 2(1), 193–218.
- Jaccard, P. (1912). The distribution of the flora in the alpine zone. *The New Phytologist* 11(2), 37–50.
- Jackson, J. E. (2004). *A User's Guide to Principal Components*. John Wiley & Sons, Inc.
- Jain, A. K., R. P. W. Duin, and J. Mao (2000). Statistical pattern recognition: A review. *IEEE Transactions on Pattern Analysis and Machine Intelligence* 22(1), 4–37.
- Karrer, B. and M. E. J. Newman (2011). Stochastic blockmodels and community structure in networks. *Physical Review E* (3) 83(1), 016107, 10.
- Kiefer, J. and J. Wolfowitz (1956). Consistency of the maximum likelihood estimator in the presence of infinitely many incidental parameters. *The Annals of Mathematical Statistics* 27, 886 – 906.
- Ko, H., S. B. Hofer, B. Pichler, K. A. Buchanan, P. J. Sjoström, and T. D. Mrsic-Flogel (2011). Functional specificity of local synaptic connections in neocortical networks. *Nature* 473(7345), 87–91.
- Laird, N. (1978). Nonparametric maximum likelihood estimation of a mixing distribution. *Journal of the American Statistical Association* 73(364), 805 – 811.
- Lee, W.-C. A., V. Bonin, M. Reed, B. J. Graham, G. Hood, K. Glattfelder, and R. C. Reid (2016). Anatomy and function of an excitatory network in the visual cortex. *Nature* 532(7599), 370–374.
- Lesperance, M. L. and J. D. Kalbfleisch (1992). An algorithm for computing the nonparametric mle of a mixing distribution. *Journal of the American Statistical Association* 87(417), 120 – 126.

- Lindsay, B. G. (1983). The geometry of mixture likelihoods: A general theory. *The Annals of Statistics* 11(1), 86–94.
- Lindsay, B. G. and M. L. Lesperance (1995). A review of semiparametric mixture models. *Journal of Statistical Planning and Inference* 47, 29–39.
- Lyzinski, V., D. L. Sussman, M. Tang, A. Athreya, and C. E. Priebe (2014). Perfect clustering for stochastic blockmodel graphs via adjacency spectral embedding. *Electronic Journal of Statistics* 8, 2905–2922.
- Lyzinski, V., M. Tang, A. Athreya, Y. Park, and C. E. Priebe (2017). Community detection and classification in hierarchical stochastic blockmodels. *IEEE Transactions on Network Science and Engineering* 4(1), 13–26.
- Malliaros, F. D. and M. Vazirgiannis (2013). Clustering and community detection in directed networks: A survey. *Physics Reports* 533(4), 95 – 142.
- Meilă, M. (2007). Comparing clusterings—an information based distance. *Journal of Multivariate Analysis*, 873–195.
- Ohyama, T., C. M. Schneider-Mizell, R. D. Fetter, J. V. Aleman, R. Franconville, M. Rivera-Alba, B. D. Mensh, K. M. Branson, J. H. Simpson, J. W. Truman, et al. (2015). A multilevel multimodal circuit enhances action selection in drosophila. *Nature* 520(7549), 633–639.
- Rissanen, J. (1978). Modeling by shortest data description. *Automatica* 14(5), 465 – 471.
- Schneider-Mizell, C. M., S. Gerhard, M. Longair, T. Kazimiers, F. Li, M. F. Zwart, A. Champion, F. M. Midgley, R. D. Fetter, S. Saalfeld, et al. (2016). Quantitative neuroanatomy for connectomics in drosophila. *Elife* 5, e12059.
- Schwarz, G. (1978). Estimating the dimension of a model. *The Annals of Statistics* 6(2), 461–464.
- Sporns, O. (2012). *Discovering the Human Connectome* (1st ed.). The MIT Press.

- Sporns, O., G. Tononi, and R. Kotter (2005). The human connectome: A structural description of the human brain. *PLoS Computational Biology* 1(4).
- Susko, E., J. D. Kalbfleisch, and J. Chen (1998). Constrained nonparametric maximum-likelihood estimation for mixture models. *Canadian Journal of Statistics* 26(4), 601–617.
- Sussman, D. L., M. Tang, D. E. Fishkind, and C. E. Priebe (2012). A consistent adjacency spectral embedding for stochastic blockmodel graphs. *Journal of the American Statistical Association* 107(499), 1119–1128.
- Sussman, D. L., M. Tang, and C. E. Priebe (2014). Consistent latent position estimation and vertex classification for random dot product graphs. *IEEE Transactions on Pattern Analysis and Machine Intelligence* 36, 48–57.
- Tang, M. and C. E. Priebe (2016). Limit theorems for eigenvectors of the normalized Laplacian for random graphs. *arXiv:1607.0123*.
- Tang, M., D. L. Sussman, and C. E. Priebe (2013). Universally consistent vertex classification for latent position graphs. *The Annals of Statistics* 41, 1406 – 1430.
- Varshney, L. R., B. L. Chen, E. Paniagua, D. H. Hall, and D. B. Chklovskii (2011). Structural properties of the caenorhabditis elegans neuronal network. *PLoS Computational Biology* 7(2), 1–21.
- Vogelstein, J. T., Y. Park, T. Ohyama, R. A. Kerr, J. W. Truman, C. E. Priebe, and M. Zlatic (2014). Discovery of brainwide neural-behavioral maps via multiscale unsupervised structure learning. *Science* 344(6182), 386–392.
- Wang, Y. (2010). Maximum likelihood computation for fitting semiparametric mixture models. *Statistics and Computing* 20, 75–86.
- Wang, Y. J. and G. Y. Wong (1987). Stochastic blockmodels for directed graphs. *Journal of the American Statistical Association* 82, 8–19.

- White, J. G., E. Southgate, J. N. Thomson, and S. Brenner (1986). The Structure of the Nervous System of the Nematode *Caenorhabditis elegans*. *Philosophical Transactions of the Royal Society of London Series B* 314, 1–340.
- Zhu, M. and A. Ghodsi (2006). Automatic dimensionality selection from the scree plot via the use of profile likelihood. *Computational Statistics and Data Analysis* 51(2), 918–930.
- Zilles, K. and K. Amunts (2010). Centenary of Brodmann’s map – conception and fate. *Nature Reviews Neuroscience* 11(2), 139–145.